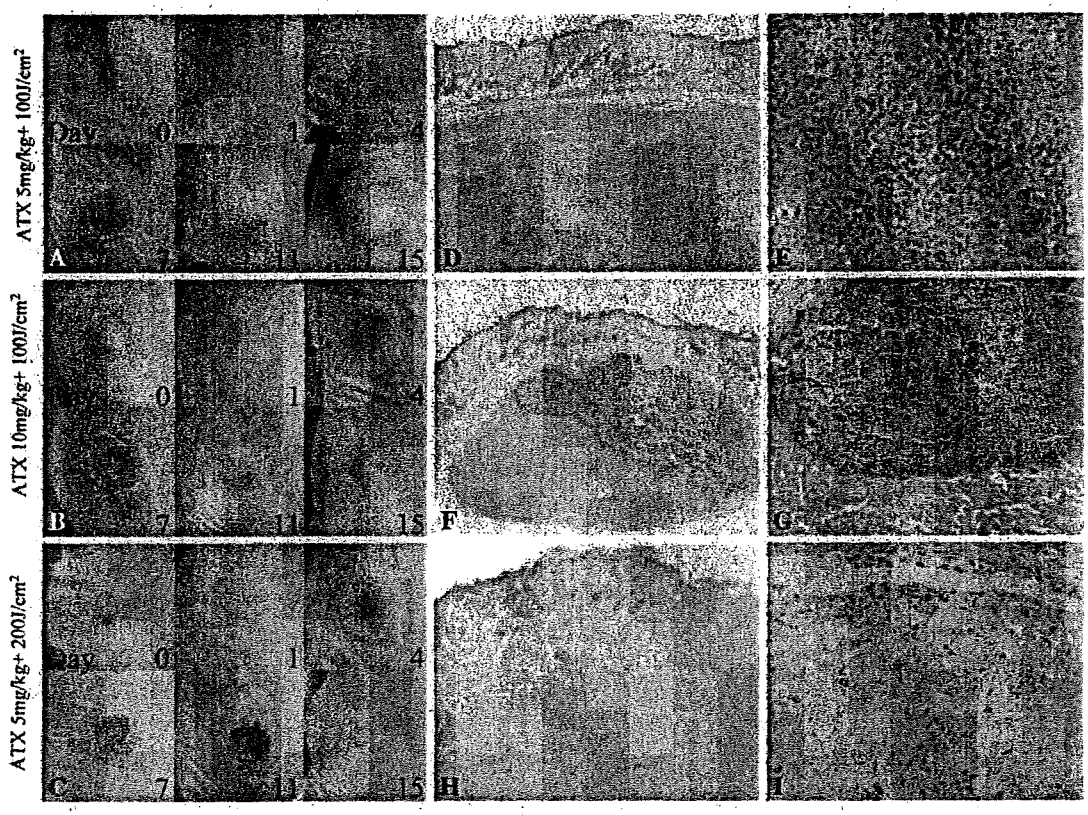

Fig. 5A–I The illustrations show the change of macroscopic findings of the tumor after (**A**) PDT with 5 mg/kg ATX-S10·Na(II) and 100 J/cm^2 laser irradiation, (**B**) 10 mg/kg ATX-S10·Na(II) and 100 J/cm^2 laser irradiation, and (**C**) 5 mg/kg ATX-S10·Na(II) and 200 J/cm^2 laser irradiation. Histologic samples with hematoxylin and eosin staining, (**D**) shown at ×4 and (**E**) × 200 magnification, were made on Day 15 after PDT with 5 mg/kg ATX-S10·Na(II) and 100 J/cm^2 laser irradiation, at (**F**) ×4 and (**G**) ×200 magnification for 10 mg/kg ATX-S10·Na(II) and 100 J/cm^2 laser irradiation, and at (**H**) ×4 and (**I**) ×200 magnification for 5 mg/kg ATX-S10·Na(II) and 200 J/cm^2 laser irradiation. (**A–C**) A dusky scan was observed at the treatment location, which thereafter gradually decreased in size and then normal skin developed. (**A**) The tumor grew gradually 11 days after PDT with 100 J/cm^2 laser irradiation. No necrotic area was seen inside the tumor on Day 15 after PDT using (**D**) 5 mg/kg ATX-S10·Na(II) injection and 100 J/cm^2 irradiation and (**E**) SYO-1 cells were all viable. Photodynamic therapy (**F, G**) using an injection of 10 mg/kg ATX-S10·Na(II) and irradiation with 100 J/cm^2 caused necrosis of the tumors, although an area of viable tumor cells remained under the necrotic area. (**H, I**) An injection of 5 mg/kg ATX-S10·Na(II) and irradiation with 200 J/cm^2 resulted in a completely necrotic area of the tumor and no viable tumor cells were observed.

indicating ATX-S10·Na(II) could cause less skin photosensitization [19]. Our data suggest ATX-S10·Na(II) was incorporated in implanted synovial sarcoma on mice until 6 hours after intravenous injection, and it was eliminated from tumor tissues less than 12 hours after injection. ATX-S10·Na(II) has been reported to be excreted rapidly, within 3 hours after administration, from normal surrounding organs such as muscles, lungs, and brain [17, 19, 21]. Prolonged light protection might not be required after administration of ATX-S10·Na(II) PDT because of its rapid clearance compared with other photosensitizers [23].

Table 1. Local control after marginal resection of the tumor with or without PDT

Treatment	Recurrence		Total
	Yes	No	
Marginal resection + PDT	2	8	10
Control (marginal resection alone)	9	1	10

PDT = photodynamic therapy.

Photodynamic therapy on SYO-1-bearing mice can inhibit tumor growth in 15 days, thus indicating PDT may be an effective therapy for synovial sarcoma. Moreover, PDT with 200 J/cm^2 irradiation showed no local recurrence after 15 days. However, SYO-1-bearing mice showed regrowth of the tumor after PDT with 100 J/cm^2 irradiation. Photodynamic therapy with lower laser irradiation therefore might not sufficiently abolish tumor cells in deep layers. Preventing local recurrence after PDT also may require higher laser irradiation. The in vivo mechanism of PDT remains controversial. ATX-S10·Na(II) was reported to produce singlet oxygen, which thus induces cell death directly [21]. Furthermore, PDT using ATX-S10·Na(II)

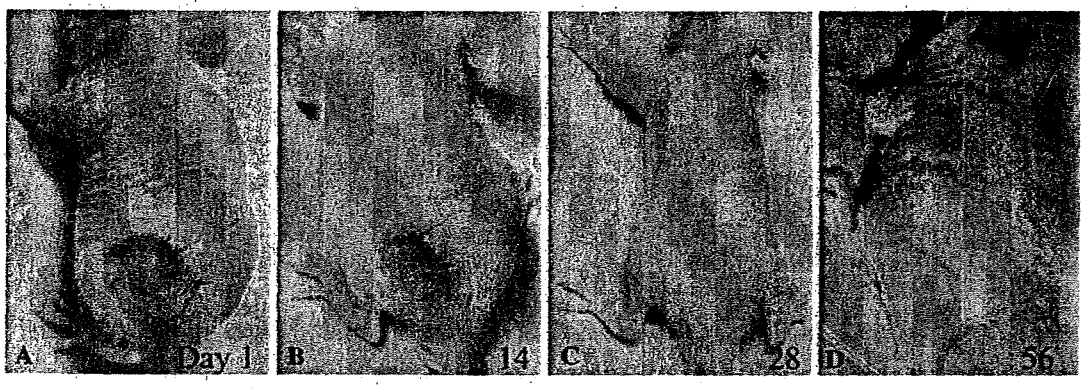

Fig. 6A–D Marginal resection followed by PDT 3 hours after an intravenous injection of 10 mg/kg ATX-S10 Na(II) was performed on the SYO-1-forming tumors. The illustrations shows the macroscopic findings of mice received marginal resection followed by PDT at (A) Day 1, (B) Day 14, (C) Day 28, and (D) Day 56 after treatment. The skin (A) in the treatment area lost its normal pink color on Day 1 after treatment. (B) A dark scab was observed approximately 2 weeks later, (C) which peeled off and finally healed with a normal appearance. (D) No tumor recurrence was observed by 56 days after this procedure.

and a diode laser was reported to have an indirect antitumor effect induced by vascular shutdown and inhibition of nutritional supply to tumor cells [20].

Musculoskeletal tumors often are located in deep layers and usually grow to greater than 5 cm in size. Photodynamic therapy alone therefore is insufficient for clinical treatment of musculoskeletal sarcomas because of the limited penetration of laser light. The maximal depth of necrosis induced by ATX-S10·Na(II) PDT is reportedly 7.9 mm in the treated tumor [17]. We developed PDT as adjuvant treatment after a marginal resection, which can preserve such adjacent critical tissues as nerves and vessels. Adjuvant PDT could eliminate residual tumor cells after a marginal resection. In our study, a marginal resection followed by adjuvant ATX-S10·Na(II) PDT in mice reduced the local recurrence rate of SYO-1-forming tumors. This suggests adjuvant ATX-S10·Na(II) PDT can be effective for the remaining residual cells after marginal resection. However, a 20% recurrence rate is not clinically acceptable. Because these local recurrences were in the peripheral area of PDT, it is possible wider irradiation or higher laser dose might have prevented local recurrence of the residual tumor cells in those areas. Kusuzaki et al. reported acridine orange PDT followed by radiotherapy suppressed tumor growth of osteosarcoma-bearing mice [15]. Jin et al. also suggested the use of a combination of PDT and sonodynamic therapy improved the tumoricidal effects in squamous cell carcinoma in mice [9]. Okunaka et al. reported the pulsed wave laser showed a higher effect of PDT than the continuous-wave laser [23]. Additional therapy such as radiotherapy and sonodynamic therapy and the use of a pulsed wave laser therefore also might reduce the risk of local tumor recurrence after ATX-S10·Na(II) PDT.

We observed the in vitro and in vivo antitumor effects of ATX-S10·Na(II) PDT on synovial sarcoma. Although additional clinical trials are necessary, our results indicated ATX-S10·Na(II) PDT may be a potentially useful treatment modality, especially as adjuvant therapy to reduce the size of the surgical margin for synovial sarcoma. Preservation of critical muscles, nerves, and vessels adjacent to tumors treated with ATX-S10·Na(II) PDT would result in a better postoperative functional outcome and improved quality of life.

Acknowledgments We thank Dr. Isao Sakata and Mr. Ryuji Asano, Photochemical Co, Ltd (Okayama, Japan), for their kind cooperation in preparing and providing ATX-S10·Na (II) and Hamamatsu Photonics KK (Hamamatsu, Japan) for providing the diode laser system. We also thank Dr. Isao Sakata for information regarding the lethal dose of ATX-S10·Na (II).

References

1. Berger AP, Steiner H, Stenzl A, Akkád T, Bartsch G, Holtl L. Photodynamic therapy with intravesical instillation of 5-aminolevulinic acid for patients with recurrent superficial bladder cancer: a single-center study. *Urology*. 2003;61:338–341.
2. Dolmans DE, Kadambi A, Hill JS, Flores KR, Gerber JN, Walker JP, Borel Rinkes IH, Jain RK, Fukumura D. Targeting tumor vasculature and cancer cells in orthotopic breast tumor by fractionated photosensitizer dosing photodynamic therapy. *Cancer Res*. 2002;62:4289–4294.
3. Dougherty TJ, Gomer CJ, Henderson BW, Jori G, Kessel D, Korbelik M, Moan J, Peng Q. Photodynamic therapy. *J Natl Cancer Inst*. 1998;90:889–905.
4. Edmonson JH, Ryan LM, Blum RH, Brooks JS, Shiraki M, Frytak S, Parkinson DR. Randomized comparison of doxorubicin alone versus ifosfamide plus doxorubicin or mitomycin, doxorubicin, and cisplatin against advanced soft tissue sarcomas. *J Clin Oncol*. 1993;11:1269–1275.
5. Fingar VH, Kik PK, Haydon PS, Cerrito PB, Tseng M, Abang E, Wieman TJ. Analysis of acute vascular damage after photodynamic therapy using benzoporphyrin derivative (BPD). *Br J Cancer*. 1999;79:1702–1708.

6. Frustaci S, Gherlinzoni F, De Paoli A, Bonetti M, Azzarelli A, Comandone A, Olmi P, Buonadonna A, Pignatti G, Barbieri E, Apice G, Zmerly H, Serraino D, Picci P. Adjuvant chemotherapy for adult soft tissue sarcomas of the extremities and girdles: results of the Italian randomized cooperative trial. *J Clin Oncol.* 2001;19:1238–1247.
7. Henderson BW, Dougherty TJ. How does photodynamic therapy work? *Photochem Photobiol.* 1992;55:145–157.
8. Hopfner M, Maaser K, Theiss A, Lenz M, Sutter AP, Kashtan H, von Lampe B, Riecken EO, Zeitz M, Scherubl H. Hypericin activated by an incoherent light source has photodynamic effects on esophageal cancer cells. *Int J Colorectal Dis.* 2003;18:239–247.
9. Jin ZH, Miyoshi N, Ishiguro K, Umemura S, Kawabata K, Yumita N, Sakata I, Takaoka K, Udagawa T, Nakajima S, Tajiri H, Ueda K, Fukuda M, Kumakiri M. Combination effect of photodynamic and sonodynamic therapy on experimental skin squamous cell carcinoma in C3H/HeN mice. *J Dermatol.* 2000;27:294–306.
10. Kato H, Furukawa K, Sato M, Okunaka T, Kusunoki Y, Kawahara M, Fukuoka M, Miyazawa T, Yana T, Matsui K, Shiraishi T, Horinouchi H. Phase II clinical study of photodynamic therapy using mono-L-aspartyl chlorin e6 and diode laser for early superficial squamous cell carcinoma of the lung. *Lung Cancer.* 2003;42:103–111.
11. Kawai A, Naito N, Yoshida A, Morimoto Y, Ouchida M, Shimizu K, Beppu Y. Establishment and characterization of a biphasic synovial sarcoma cell line, SYO-1. *Cancer Lett.* 2004;204:105–113.
12. Kriegmair M, Baumgartner R, Lumper W, Waidelich R, Hofstetter A. Early clinical experience with 5-aminolevulinic acid for the photodynamic therapy of superficial bladder cancer. *Br J Urol.* 1996;77:667–671.
13. Kusuzaki K, Aomori K, Suginoshita T, Minami G, Takeshita H, Murata H, Hashiguchi S, Ashihara T, Hirasawa Y. Total tumor cell elimination with minimum damage to normal tissues in musculoskeletal sarcomas following photodynamic therapy with acridine orange. *Oncology.* 2000;59:174–180.
14. Kusuzaki K, Minami G, Takeshita H, Murata H, Hashiguchi S, Nozaki T, Ashihara T, Hirasawa Y. Photodynamic inactivation with acridine orange on a multidrug-resistant mouse osteosarcoma cell line. *Jpn J Cancer Res.* 2000;91:439–445.
15. Kusuzaki K, Murata H, Matsubara T, Miyazaki S, Okamura A, Seto M, Matsumine A, Hosoi H, Sugimoto T, Uchida A. Clinical trial of photodynamic therapy using acridine orange with/without low dose radiation as new limb salvage modality in musculoskeletal sarcomas. *Anticancer Res.* 2005;25:1225–1235.
16. Lou PJ, Jager HR, Jones L, Theodossy T, Bown SG, Hopper C. Interstitial photodynamic therapy as salvage treatment for recurrent head and neck cancer. *Br J Cancer.* 2004;91:441–446.
17. Masumoto K, Yamada I, Tanaka H, Fujise Y, Hashimoto K. Tissue distribution of a new photosensitizer ATX-S10Na(II) and effect of a diode laser (670 nm) in photodynamic therapy. *Lasers Med Sci.* 2003;18:134–138.
18. McCaughan JS Jr. Survival after photodynamic therapy to nonpulmonary metastatic endobronchial tumors. *Lasers Surg Med.* 1999;24:194–201.
19. Mori M, Kuroda T, Obana A, Sakata I, Hirano T, Nakajima S, Hikida M, Kumagai T. In vitro plasma protein binding and cellular uptake of ATX-S10(Na), a hydrophilic chlorin photosensitizer. *Jpn J Cancer Res.* 2000;91:845–852.
20. Mori M, Sakata I, Hirano T, Obana A, Nakajima S, Hikida M, Kumagai T. Photodynamic therapy for experimental tumors using ATX-S10(Na), a hydrophilic chlorin photosensitizer, and diode laser. *Jpn J Cancer Res.* 2000;91:753–759.
21. Nakajima S, Sakata I, Hirano T, Takemura T. Therapeutic effect of interstitial photodynamic therapy using ATX-S10(Na) and a diode laser on radio-resistant SCCVII tumors of C3H/He mice. *Anticancer Drugs.* 1998;9:539–543.
22. Obana A, Gohto Y, Kaneda K, Nakajima S, Takemura T, Miki T. Selective occlusion of choroidal neovascularization by photodynamic therapy with a water-soluble photosensitizer, ATX-S10. *Lasers Surg Med.* 1999;24:209–222.
23. Okunaka T, Kato H, Konaka C, Sakai H, Kawabe H, Aizawa K. A comparison between argon-dye and excimer-dye laser for photodynamic effect in transplanted mouse tumor. *Jpn J Cancer Res.* 1992;83:226–231.
24. Oseroff AR, Shieh S, Frawley NP, Cheney R, Blumenson LE, Pivnick EK, Bellnier DA. Treatment of diffuse basal cell carcinomas and basaloid follicular hamartomas in nevoid basal cell carcinoma syndrome by wide-area 5-aminolevulinic acid photodynamic therapy. *Arch Dermatol.* 2005;141:60–67.
25. Ragunath K, Krasner N, Raman VS, Haqqani MT, Phillips CJ, Cheung I. Endoscopic ablation of dysplastic Barrett's oesophagus comparing argon plasma coagulation and photodynamic therapy: a randomized prospective trial assessing efficacy and cost-effectiveness. *Scand J Gastroenterol.* 2005;40:750–758.
26. Skyrme RJ, French AJ, Datta SN, Allman R, Mason MD, Matthews PN. A phase-1 study of sequential mitomycin C and 5-aminolaevulinic acid-mediated photodynamic therapy in recurrent superficial bladder carcinoma. *BJU Int.* 2005;95:1206–1210.
27. Takahashi H, Itoh Y, Nakajima S, Sakata I, Iizuka H. A novel ATX-S10(Na) photodynamic therapy for human skin tumors and benign hyperproliferative skin. *Photodermatol Photoimmunol Photomed.* 2004;20:257–265.
28. Takahashi H, Nakajima S, Sakata I, Ishida-Yamamoto A, Iizuka H. Photodynamic therapy using a novel photosensitizer, ATX-S10(Na): comparative effect with 5-aminolevulinic acid on squamous cell carcinoma cell line, SCC15, ultraviolet B-induced skin tumor, and phorbol ester-induced hyperproliferative skin. *Arch Dermatol Res.* 2005;296:496–502.
29. Wang CP, Chang YL, Chen CT, Yang TH, Lou PJ. Photodynamic therapy with topical 5-aminolevulinic acid as a post-operative adjuvant therapy for an incompletely resected primary nasopharyngeal papillary adenocarcinoma: a case report. *Lasers Surg Med.* 2006;38:435–438.
30. Woodburn KW, Fan Q, Kessel D, Wright M, Mody TD, Hemmi G, Magda D, Sessler JL, Dow WC, Miller RA, Young SW. Phototherapy of cancer and atheromatous plaque with texaphyrins. *J Clin Laser Med Surg.* 1996;14:343–348.
31. Yamamoto J, Hirano T, Li S, Koide M, Kohno E, Inenaga C, Tokuyama T, Yokota N, Yamamoto S, Terakawa S, Namba H. Selective accumulation and strong photodynamic effects of a new photosensitizer, ATX-S10.Na (II), in experimental malignant glioma. *Int J Oncol.* 2005;27:1207–1213.
32. Yang JC, Chang AE, Baker AR, Sindelar WF, Danforth DN, Topalian SL, DeLaney T, Glatstein E, Steinberg SM, Merino MJ, Rosenberg SA. Randomized prospective study of the benefit of adjuvant radiation therapy in the treatment of soft tissue sarcomas of the extremity. *J Clin Oncol.* 1998;16:197–203.
33. Zeitouni NC, Shieh S, Oseroff AR. Laser and photodynamic therapy in the management of cutaneous malignancies. *Clin Dermatol.* 2001;19:328–338.

Langmuir

Subscriber access provided by OKAYAMA UNIV

Article

Microcapsules with Macroholes Prepared by the Competitive Adsorption of Surfactants on Emulsion Droplet Surfaces

Eiji Kamio, Satoshi Yonemura, Tsutomu Ono, and Hidekazu Yoshizawa

Langmuir, **2008**, 24 (23), 13287-13298• DOI: 10.1021/la800758d • Publication Date (Web): 29 July 2008

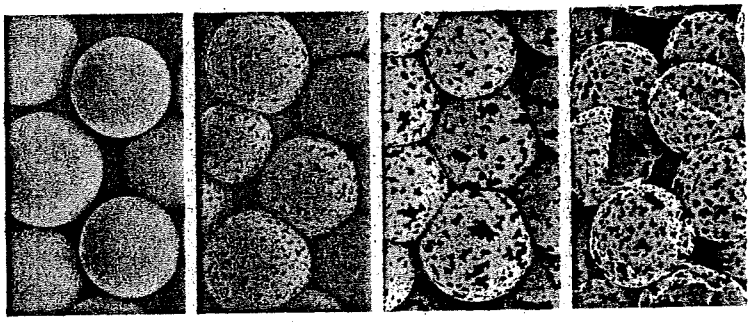

Microcapsules with Macroholes Prepared by the Competitive Adsorption of Surfactants on Emulsion Droplet Surfaces

Eiji Kamio, Satoshi Yonemura, Tsutomu Ono,* and Hidekazu Yoshizawa

Department of Environmental Chemistry and Materials, Okayama University, 3-1-1 Tsushima-naka, Okayama-shi, Okayama 700-8530, Japan

Received June 23, 2007. Revised Manuscript Received June 4, 2008

We demonstrate a simple, unique method for preparing microcapsules with holes in their shells. Cross-linked polymelamine microcapsules are prepared by the phase-separation method. The holey shell of each microcapsule is synthesized on the surface of an oil-in-water (O/W) emulsion droplet where a water-soluble polymeric surfactant and an oil-soluble surfactant are competitively adsorbed. The water-soluble polymeric surfactant provides a reaction site for shell formation. The oil-soluble surfactant molecules seem to self-assemble while the shells are being formed, so holes appear where they assemble. The critical degree of surface coverage of an emulsion droplet by the water-soluble polymeric surfactant needed to form the holey shells is determined to be 0.90 from theoretical calculations in which competitive adsorption is considered. Theoretical consideration suggests that the size and quantity of the holes in the microcapsule shells are controlled by the composition of the surfactants adsorbed on the surface of an emulsion droplet. This theoretical consideration is confirmed by experiments. The prepared microcapsule with controllable macroholes in its shell has the potential to be used for controlled release applications and can be used to fabricate a microcapsule that encapsulates hydrophilic compounds.

Introduction

Materials with well-defined structures in the submicrometer range have attracted increasing interest in recent years. Hollow particles such as microcapsules and nanocapsules are of particular interest because of their potential for encapsulating vast quantities of large guest materials within their empty cores. Such hollow materials could be useful in applications in areas as diverse as biological chemistry, synthesis, and catalysis. Several microencapsulation methods have subsequently been developed and applied to the fields in which they are used today. Microcapsules with a variety of functions can be produced by using different microencapsulation methods, such as coacervation, interfacial polymerization, solvent evaporation, and phase separation. In fact, a multitude of different applications have already been proposed for microcapsules, such as microenvironments for catalyst reactions,[1,2] drug carriers,[3,4] protective microcontainers for proteins[5] and cells,[6,7] bioreactors,[8−10] self-healing materials,[11] and electrophoretic inks.[12,13]

The fabrication of hollow spheres with complex, specific structures is currently of considerable scientific and technological interest. Modifying the pores in the shell of a hollow sphere is an interesting structural design idea. For example, Yamaguchi and co-workers prepared microcapsules with porous shells by the conventional interfacial polymerization method and then filled the pores with poly(*N*-isopropylacrylamide) or a copolymer of *N*-isopropylacrylamide and acrylic acid using the plasma-graft polymerization method.[14] By modifying the pores with environment-responsive polymers, they converted the microcapsules into environment-responsive reactors. In another interesting example, Xia and co-workers prepared polymeric microsheres, named "microscale fish bowls", where each one had a single hole in its shell that was formed by different two processes: (1) swelling a polymer particle followed by freezing and solvent evaporation and (2) preparing a polymer emulsion followed by freezing and solvent evaporation.[15] They also demonstrated that the single hole in the shell was closed by thermal annealing or solvent treatment. Before the hole in the shell was closed, different types of materials were easily and quickly loaded in the microscale fish bowl through the large hole. In addition, Yin and Yates also prepared the microscale fish bowl to fabricate a microcapsule enclosing a hydrophilic core.[16] The microscale fish bowl was immersed in water to load a water-soluble compound through the single hole, and then the hole was closed by exposing the microscale fish bowl to a second swelling solvent. Such microcapsules with hydrophilic cores should be useful in controlled-release applications. The concept underlying the modification of shells of a presynthesized hollow microshere is straightforward and practical. In this concept, the presynthesized

* To whom correspondence should be addressed. Tel/Fax: +81-86-251-8908. E-mail: tono@cc.okayama-u.ac.jp.

(1) Ren, N.; Yang, Y.-H.; Zhang, Y.-H.; Wang, Q.-R.; Tang, Y. *J. Catal.* **2007**, *246*, 215–222.
(2) Poe, S. L.; Kobaslija, M.; McQuade, D. T. *J. Am. Chem. Soc.* **2006**, *128*, 15586–15587.
(3) Zhao, Q.; Han, B.; Wang, Z.; Gao, C.; Peng, C.; Shen, J. *Nanomed.: Nanotechnol., Biol., Med.* **2007**, *3*, 63–74.
(4) Wang, S.-B.; Xu, F.-H.; He, H.-S.; Weng, L.-J. *Macromol. Biosci.* **2005**, *5*, 408–414.
(5) Shchukin, D. G.; Shutava, T.; Shchukina, E.; Sukhorukov, G. B.; Lvov, Y. M. *Chem. Mater.* **2004**, *16*, 3446–3451.
(6) Baruch, L.; Machluf, M. *Biopolymers* **2006**, *82*, 570–579.
(7) Sakai, S.; Hashimoto, I.; Kawakami, K. *Biotechnol. Bioeng.* **2008**, *99*, 235–243.
(8) Quek, C.-H.; Li, J.; Sun, T.; Chan, M. L. H.; Mao, H.-Q.; Gan, L. M.; Leong, K. W.; Yu, H. *Biomaterials* **2004**, *25*, 3531–3540.
(9) Yu, A.; Gentle, I.; Lu, G.; Caruso, F. *Chem. Commun.* **2006**, *2150*, 2152.
(10) Wyss, A.; von Stockar, U.; Marison, I. W. *Biotechnol. Bioeng.* **2006**, *93*, 28–39.
(11) White, S. R.; Sottos, N. R.; Geubelle, P. H.; Moore, J. S.; Kessler, M. R.; Sriram, S. R.; Brown, E. N.; Viswanathan, S. *Nature* **2001**, *409*, 794–797.
(12) Comiskey, B.; Albert, J. D.; Yoshizawa, H.; Jacobson, J. *Nature* **1998**, *394*, 253–255.
(13) Wang, J.; Zhao, X.; Guo, H.; Zheng, Q. *Langmuir* **2004**, *20*, 10845–10850.
(14) (a) Chu, L.-Y.; Park, S.-H.; Yamaguchi, T.; Nakao, S. *Langmuir* **2002**, *18*, 1856–1864. (b) Akamatsu, K.; Yamaguchi, T. *Ind. Eng. Chem. Res.* **2007**, *46*, 124–130.
(15) (a) Im, S. H.; Jeong, U.; Xia, Y. *Nat. Mater.* **2005**, *4*, 671–675. (b) Jeong, U.; Im, S. H.; Camargo, P. H. C.; Kim, J. H.; Xia, Y. *Langmuir* **2007**, *23*, 10968–10975.
(16) Yin, W.; Yates, M. Z. *Langmuir* **2008**, *24*, 701–708.

10.1021/la800758d CCC: $40.75
Published on Web 07/29/2008

hollow microshere is used as a template for fabricating an advanced microcapsule. Therefore, the shell geometry as well as the shell material of the presynthesized hollow microshere significantly affects the function of the modified microcapsule. That is to say, controlling the shell geometry, such as the porosity and pore diameter, of the presynthesized hollow microsphere is one of the key issues. Tailoring the composition and structure of shells in the submicrometer or nanometer range may lead to new properties for microcapsules and hence new applications.

Some interesting investigations have recently been carried out to create specific pores of nanometer size and to form micrometer- or submicrometer-sized macroholes. Wang et al. prepared a microcapsule with straight pores in the shell by sol−gel phase inversion followed by the dissolving of the dense skin layer.[17] The microcapsule was utilized as a carrier for immobilizing microbial cells. Lavergne et al. prepared PMMA microcapsules with well-defined craters (pores and holes) in their shells by the solvent evaporation method.[18] The craters, pores, and holes in the microcapsule shells were formed by the protrusion of oil, which stabilized water droplets, into the polymer phase. Fujiwara et al. synthesized silica microcapsules with nanoscale macroholes in their shells.[19] They applied the transport phenomenon of a polymer through the oil phase of a W/O/W (water/oil/water) emulsion to create the nanomacroholes. Han et al. synthesized poly(*o*-methoxyaniline) hollow microspheres where each one had a single hole in its surface.[20] The hole in the shell of the hollow microsphere was formed by the diffusion flux of monomers, and its size could be controlled by adjusting the concentration of monomers. Ma et al. prepared microcapsules by the suspension polymerization method in which hexadecane was enclosed and poly(styrene-*co*-*N*,*N*-dimethylaminoethyl methacrylate) was used as the wall material.[21] They prepared microcapsules, each with a single hole in its wall, by controlling the monomer conversion and the amount of hexadecane. The hole in the capsule wall was formed by controlling the interfacial tension between the hexadecane phase and water and that between the polystyrene phase and water. Chen et al. also fabricated a polymeric hollow sphere with a single hole in its shell.[22] They prepared the polystyrene hollow microsphere with a hole by interface-initiated emulsion polymerization in the presence of isooctane. They used cumyl hydroperoxide with Fe^{2+} as the redox initiator to ensure that the reactions of the primary radicals took place only at the oil/water interface. An interesting microcapsule with well-defined macroholes was presented by Dinsmore et al.[23] They used a colloidosome as a template for fabricating a microcapsule with a selectively permeable shell. They first fabricated a colloidosome by utilizing the adsorption property of polymeric colloidal particles onto an emulsion droplet. The adsorbed particles were then locked together by sintering the polymeric particles at a temperature somewhat higher than the glass-transition temperature of the polymer. Another interesting method for fabricating a hollow polymer particle with a hole in its shell was demonstrated by Minami et al.[24] They prepared hollow polymer particles where each one had a single hole in its polydivinylbenzene shell as a result of the self-assembling of phase-separated polymer method (named SaPSeP method) in the presence of sodium dodecyl sulfate (SDS). Their strategy for preparing hollow polymer particles, each with a hole in its shell, was unique and elegant. They used the self-assembly of polydivinylbenzene microgels at the interface of core droplets in the presence of SDS. The self-assembly of polydivinylbenzene microgels was affected by the adsorption of SDS at the interface. A hole (or holes) was formed in the shell at places where the SDS molecules had assembled and the adsorption of microgels was insufficient.

The self-assembly of surfactants and polymers is a valuable tool for tailoring the structure of microcapsule shells. It provides compartmentalization on the nanometer scale, and the sites can act as structural templates for holes in microcapsule shells. In the study reported here, we used this self-assembly strategy to synthesize polymeric microcapsules with macroholes in their shells. We prepared the microcapsules by the phase-separation method because we have been investigating the shell-formation mechanism of cross-linked polyamino resin microcapsules

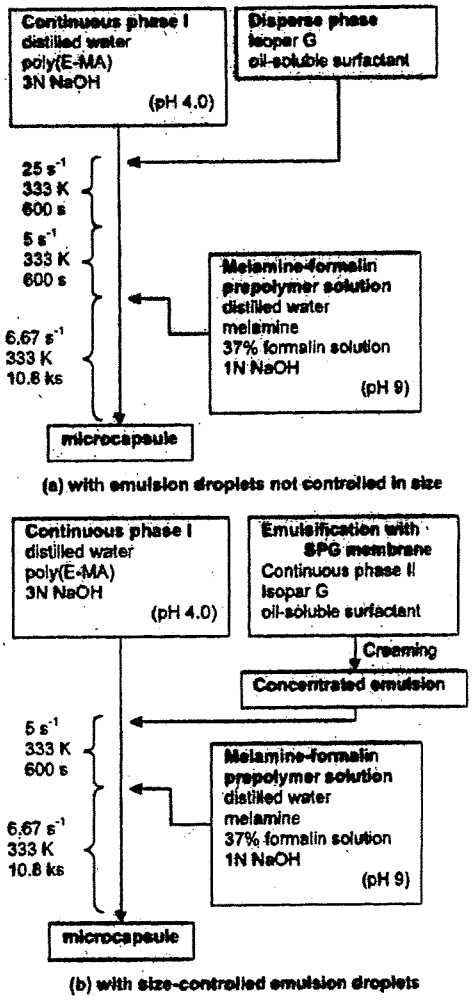

Figure 1. Protocol for preparing cross-linked polymelamine microcapsules encapsulating an oily core in which an oil-soluble surfactant was dissolved. The size distributions of the emulsion droplets were (a) polydisperse and (b) uniform in size, so in part a only some of the microcapsules in the same batch prepared according to this process had macroholes in their shells, but in part b, all of them did. To check the theory proposed in this work and to prepare microcapsules with macroholes of the same quality, it was necessary to use emulsion droplets of a uniform size.

(17) (a) Wang, G.-J.; Chu, L.-Y.; Chen, W.-M.; Zhou, M.-Y. *J. Membr. Sci.* **2005**, *252*, 279–284. (b) Wang, G.-J.; Chu, L.-Y.; Zhou, M.-Y.; Chen, W.-M. *J. Membr. Sci.* **2006**, *284*, 301–312.

(18) Lavergne, F.-M.; Cot, D.; Ganachaud, F. *Langmuir* **2007**, *23*, 6744–6753.

(19) Fujiwara, M.; Shiokawa, K.; Sakakura, I.; Nakahara, Y. *Nano Lett.* **2006**, *6*, 2925–2928.

(20) Han, J.; Song, G.; Guo, R. *Chem. Mater.* **2007**, *19*, 973–975.

(21) Ma, G. H.; Su, Z. G.; Omi, S.; Sundberg, D.; Stubbs, J. *J. Colloid Interface Sci.* **2003**, *266*, 282–294.

(22) Chen, Y.; Qian, Z.; Zhang, Z. *Chem. Lett.* **2007**, *36*, 944–945.

(23) Dinsmore, A. D.; Hsu, M. F.; Nikolaides, M. G.; Marquez, M.; Bausch, A. R.; Weitz, D. A. *Science* **2002**, *298*, 1006–1009.

(24) Minami, H.; Kobayashi, H.; Okubo, M. *Langmuir* **2005**, *21*, 5655–5658.

Table 1. Preparation Conditions for Cross-Linked Polymelamine Microcapsules with Polydisperse Emulsion Droplets in Which Oil-Soluble Surfactant Was Dissolved

	total amount (g)	content	amount (g)
continuous phase I	100.0	distilled water (+ NaOH)	97.5
		poly(E-MA)	2.5
disperse phase	15.0	Isopar G + oil-soluble surfactant[a,b]	15.0
melamine–formalin prepolymer solution	50.0	melamine	5.0
		37% formaline solution	12.5
		distilled water (+ NaOH)	32.5

[a] Concentration of oil-soluble surfactant in the disperse phase: 0.01, 0.1, 0.5, 0.8, 1.0, or 5.0 wt %. [b] Dissolved oil-soluble surfactant: Solsperse17000 or SPAN85.

Table 2. Preparation Conditions for Cross-Linked Polymelamine Microcapsules with Size-Controlled Emulsion Droplets Containing Solsperse17000 Prepared by SPG Membrane Emulsification

Emulsion Droplets with Different Average Diameters and Constant Solsperse17000 Concentration, with Conditions the Same as in Figure 8

	total amount (g)	content	amount (g)
continuous phase I	94.5	distilled water (+ NaOH)	92.0
		poly(E-MA)	2.5
concentrated emulsion[a]	15.5	Isopar G	9.75
		Solsperse17000	0.011
		continuous phase II	5.74
melamine–formalin prepolymer solution	50.0	melamine	5.0
		37% formaline solution	12.5
		distilled water (+ NaOH)	32.5

Emulsion Droplets with Constant Average Diameter and Different Solsperse17000 Concentrations, with Conditions the Same as in Figure 9

	total amount (g)	content	amount (g)[c] (a)	(b)
continuous phase I	94.5	distilled water (+ NaOH)	92.0	92.0
		poly(E-MA)	2.5	2.5
concentrated emulsion[b]	15.5	Isopar G	9.75	9.73
		Solsperse17000	0.015	0.029
		continuous phase II	5.74	5.74
melamine–formalin prepolymer solution	50.0	melamine	5.0	5.0
		37% formaline solution	12.5	12.5
		distilled water (+ NaOH)	32.5	32.5

[a] Average diameters of emulsion droplets were 5.5, 16.0, and 23.0 μm. Continuous phase II: 1.0 wt % SDS solution. [b] Average diameter of emulsion droplets was 8.0 μm. Continuous phase II: 1.0 wt % SDS solution. [c] Panels (a) and (b) correspond to those in Figure 9.

prepared by the phase-separation method in our laboratory.[25] We found that the water-soluble polymeric surfactant, which was added in the continuous phase, adsorbed on the surface of an emulsion droplet and provided a foothold for the reaction to form the microcapsule shell. We therefore expected that microcapsules with macroholes could be prepared when the phase-separation method was applied in the presence of an additional surfactant that would self-assemble while the shell was being formed and provide sites where macroholes could form. We examined the preparation of microcapsules according to this strategy. We also tried to explain the resulting phenomenon from a theoretical viewpoint and to tailor the structure of the microcapsule shell according to theoretical considerations. In addition to reporting these studies, we describe the potential of microcapsules with tailored holes in their shells for controlled release applications and as templates for fabricating advanced microcapsules.

Experimental Section

Materials. Melamine was used for the monomer, and 37% formalin solution was used for the condensing agent. SDS and polyvinyl pyrrolidone (PVP) were used as an emulsion stabilizer in the emulsification process using a Shirasu porous glass (SPG) membrane. Sodium hydroxide was used to adjust the pH of the continuous phase in the microencapsulation process. They were analytical-grade reagents purchased from Wako Pure Chemical Industries, Ltd. The polymeric surfactant, poly(ethylene-*alt*-maleic anhydride) (poly(E-MA), weight-average molecular weight M_w = 100 000–500 000 g/mol) was purchased from Aldrich. It was dissolved in distilled water at 363 K under vigorous agitation. It should be noted that almost all maleic anhydride units of poly(E-MA) were hydrolyzed to maleic acid units. Therefore, poly(E-MA) acted as a hydrophilic surfactant. Solsperse17000 and Sorbitan trioleate (SPAN85), which are oil-soluble surfactants, were used as additional surfactants. Solseperse17000 was kindly supplied by Lubizol Japan Ltd. Its weight-average molecular weight M_w was measured by gel permeation chromatography (HLC8120, Tosoh, GPC) on the basis of polystyrene standards with tetrahydrofuran as an eluent and was determined to be 4140 g/mol. SPAN85 was purchased from Aldrich. Its molecular weight was 957.5 g/mol. These oil-soluble surfactants were not distributed in an aqueous phase. The aim of using oil-soluble surfactants as additional surfactants was to prevent them from interacting with poly(E-MA) or melamine–formaldehyde prepolymer in the continuous phase while the microcapsule shells were being formed. Isopar G was used as the solvent in the disperse phase enclosed in the microcapsules. It was purchased from Exxon Mobil Co. The specific gravity of Isopar G is 7.49 × 10^5 g/m^3. Oil blue N and oil red O were used as oil-soluble dyes to confirm the elution of the core material from the microcapsules. They were purchased from Aldrich. Ethanol was used to elute the core material from the microcapsules. It was an analytical-grade reagent. Reactive blue 160 was used as a water-soluble dye. They were purchased from Wako Pure Chemical Industries. All chemicals were used as received.

Preparation of Cross-Linked Polymelamine Microcapsules. Cross-linked polymelamine microcapsules were prepared using the following procedure. An adequate amount of poly(E-MA) was dissolved in ultrapure water. (The resulting aqueous solution is called continuous phase I hereafter.) The pH of continuous phase I was about 2 and was adjusted to 4.0 by using a 3 × 10^3 mol/m^3 NaOH aqueous solution. The disperse phase was prepared by dissolving the required amount of oil-soluble surfactant in Isopar G. The O/W emulsions were prepared by two different processes: (1) mixing continuous phase I and the disperse phase at 25 s^{-1} for 600 s to prepare the emulsion without size control and (2) SPG membrane emulsification, as described in the next section, to prepare a size-controlled emulsion. In both cases, the emulsion was stirred for 600 s at 333 K while being agitated at 5 s^{-1}. Microencapsulation then began with the addition of the melamine–formalin prepolymer solution, which was prepared separately. The prepolymer solution

(25) (a) Yoshizawa, H.; Kamio, E.; Hirabayashi, N.; Jacobson, J.; Kitamura, Y. *J. Microencapsulation* **2004**, *21*, 241–249. (b) Yoshizawa, H.; Kamio, E.; Kobayashi, E.; Jacobson, J.; Kitamura, Y. *J. Microencapsulation* **2007**, *24*, 349–357.

Table 3. Preparation Conditions for Cross-Linked Polymelamine Microcapsules with Size-Controlled Emulsion Droplets Containing SPAN85 Prepared by SPG Membrane Emulsification

Emulsion Droplets with Constant Average Diameter and Different SPAN85 Concentrations with Conditions the Same as in Figure 10

			amount (g)[b]			
	total amount (g)	content	(a)	(b)	(c)	(d)
continuous phase I	94.5	distilled water (+ NaOH)	92.0	92.0	92.0	92.0
		poly(E-MA)	2.5	2.5	2.5	2.5
concentrated emulsion[a]	15.5	Isopar G	9.72	9.71	9.70	9.67
		SPAN85	0.042	0.049	0.059	0.088
		continuous phase II	5.74	5.74	5.74	5.74
melamine–formalin prepolymer solution	50.0	melamine	5.0	5.0	5.0	5.0
		37% formaline solution	12.5	12.5	12.5	12.5
		distilled water (+ NaOH)	32.5	32.5	32.5	32.5

Different Poly(E-MA) Concentrations, with Conditions the Same as in Figure 11

			amount (g)[d]		
	total amount (g)	content	(a)	(b)	(c)
continuous phase I	94.5	distilled water (+ NaOH)	92.0	91.5	89.5
		poly(E-MA)	2.5	3.0	5.0
concentrated emulsion[c]	15.5	Isopar G	9.71	9.71	9.71
		SPAN85	0.049	0.049	0.049
		continuous phase II	5.74	5.74	5.74
melamine–formalin prepolymer solution	50.0	melamine	5.0	5.0	5.0
		37% formaline solution	12.5	12.5	12.5
		distilled water (+ NaOH)	32.5	32.5	32.5

[a] Average diameter of emulsion droplets was 32.3 μm. Continuous phase II: distilled water containing SDS (0.1 wt %) and PVP (3.0 wt %). [b] Panels (a)–(c) correspond to those in Figure 11. [c] Average diameter of emulsion droplets was 18.3 μm. Continuous phase II: distilled water containing SDS (0.1 wt %) and PVP (3.0 wt %). [d] Panels (a)–(d) correspond to those in Figure 10.

was prepared as follows: 5.0 g of melamine, 12.5 g of formalin solution, and 32.5 g of distilled water with its pH adjusted to 9 by using a 1×10^3 mol/m^3 NaOH aqueous solution were mixed and stirred at 333 K for 900 s. The temperature was kept constant at 333 K during microencapsulation, which was carried out for 10.8 ks with agitation at 6.67 s^{-1}. After 10.8 ks, the prepared microcapsules were collected and washed with distilled water. The morphology of the microcapsules was observed using a field-emission scanning electron microscope (FE-SEM S-4700, Hitachi). The process and conditions for preparing the cross-linked polymelamine microcapsules using emulsion droplets whose sizes were not controlled are shown in Figure 1a and Table 1, respectively. The process for the emulsion droplets whose size was controlled by SPG membrane emulsification is shown in Figure 1b. The conditions corresponding to Figure 1b for Solsperse17000 and SPAN85 are summarized in Tables 2 and 3, respectively.

SPG Membrane Emulsification. SPG membranes are highly porous glass and are made of deposits of volcanic ash and sand. They have a large number of uniform micrometer-sized pores. An SPG membrane with the required pore size can be selected to prepare monodisperse emulsion droplets with the required diameter.[26] We used tubular SPG membranes with pores of different sizes. They were purchased from SPG Technology Co. Ltd. An SPG-membrane-emulsification module (SPG mini-kit, SPG Technology Co. Ltd.) was used to prepare a monodisperse O/W emulsion. The continuous phase of the emulsification process (called continuous phase II hereinafter) was first introduced inside the tubular SPG membrane. For continuous phase II, we used a 1 wt % SDS solution for the preparation of the emulsion droplets containing Solsperse17000 and an aqueous mixture of 0.1 wt % SDS and 3.0 wt % PVP for the droplets containing SPAN85.[26d,e] Continuous phase II was circulated inside the tubular SPG membrane using a pump. The disperse phase was then inserted into continuous phase II from outside the SPG membrane by compressed N_2 gas at a pressure that was kept constant during the emulsification process. The resulting emulsion was continuously circulated inside the tubular SPG membrane while the disperse phase was being inserted. When the required amount of disperse phase had been emulsified, the N_2 gas was diverted to stop the disperse phase from being inserted, and the emulsion was removed from the emulsification module. We subsequently decreased the SDS and PVP concentrations in the continuous phase with the following procedure to prevent any interactions between poly(E-MA) or melamine–formaldehyde prepolymer and SDS or PVP during microencapsulation. We first poured the emulsion obtained by SPG membrane emulsification into a separation funnel and creamed it. The emulsion was settled until the oil droplets floated upward and concentrated in the upper layer. The lower phase, in which no oil droplets were present, was discarded. The upper layer (concentrated emulsion) was then collected and dispersed in continuous phase I. This treatment reduced the SDS concentration in the mixture of continuous phase I, continuous phase II, and the melamine–formalin prepolymer solution (the mixture is called continuous phase III hereafter) to about 1/25 of that in continuous phase II. A detailed description of the SPG membrane emulsification process followed by microencapsulation is given in the Supporting Information (Figure S1).

Interfacial Tension Measurement. The interfacial tension between the oil phase (disperse phase) having different concentrations of the oil-soluble surfactant and water and between Isopar G and continuous phase I of different poly(E-MA) concentrations was measured with a Wilhelmy plate interfacial tension meter (K100, Krüss). The interfacial tension was measured until it plateaued (i.e., the adsorption of the surfactant on the interface reached equilibrium). Experiments were carried out at 298 K.

Release of Core Material from the Microcapsules. The release property of an encapsulated material from the microcapsules was

(26) (a) Nakashima, T.; Shimizu, M. *Kagaku Kogaku Ronbunshu* **1989**, *15*, 645–651. (b) Yoshizawa, H.; Ohta, H.; Maruta, M.; Uemura, Y.; Ijichi, K.; Hatate, Y. *J. Chem. Eng. Jpn.* **1996**, *29*, 1027–1029. (c) Supsakulchai, A.; Ma, G. H.; Nagai, M.; Omi, S. *J. Microencapsulation* **2002**, *19*, 425–450. (d) Ma, G. H.; Sone, H.; Omi, S. *Macromolecules* **2004**, *37*, 2954–2964. (e) Kamio, E.; Kato, A.; Yonemura, S.; Ono, T.; Yoshizawa, H. *Colloid Polym. Sci.* **2008**, *286*, 787–793.

Table 4. Summary of Microcapsule Formation[a]

	oil-soluble surfactant (wt %)					
	0.01	0.1	0.5	0.8	1	5
Solsperse17000	○	△	×	×	×	×
SPAN85	○	○	○	△	△	×

[a] Microcapsule was prepared (○) or not prepared (×) in holes (△).

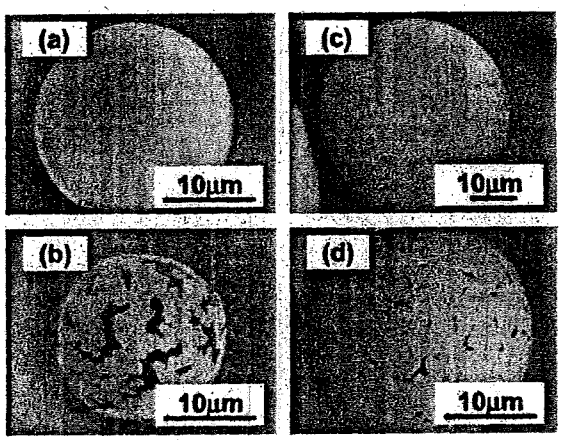

Figure 2. Cross-linked polymelamine microcapsules prepared with the disperse phase in which an oil-soluble surfactant was dissolved. The oil-soluble surfactants used were (a and b) Solsperse17000 and (c and d) SPAN85. Concentrations of Solsperse17000 were (a) 0.01 and (b) 0.12 wt %. Concentrations of SPAN85 were (c) 0.1 and (d) 0.8 wt %.

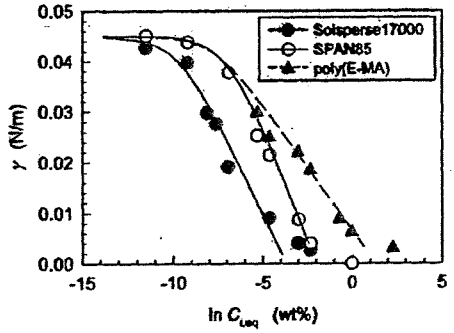

Figure 3. Relationship between interfacial tension and concentration of surfactant used in this study. Solid and broken lines are the results calculated using eq 10.

investigated as follows. Prepared microcapsules with Isopar G containing oil blue N as their core were collected by filtration. Microcapsules (2.0 g) in the wet state were weighed and poured into 1.0×10^{-4} m^3 of ethanol while being stirred at 5.0 s^{-1}. The temperature was kept constant at 298 K during the experiment, which was carried out for 1.8 ks with agitation at 5.0 s^{-1}. At the desired intervals, 1×10^{-6} m^3 of the suspension was collected in a syringe, and 0.5×10^{-6} m^3 of the continuous phase was immediately separated from the microcapsules by being passed through a filter. The visible-light absorbance of the sample at 643 nm was measured using a spectrophotometer (U-2000A, Hitachi), and the concentration of oil blue N was determined.

Results and Discussion

Fabrication of Microcapsules with Holey Shells. The results for microencapsulation according to the protocol in Figure 1a are summarized in Table 4. Typical SEM images of the prepared microcapsules are shown in Figure 2. Microcapsules with complete, smooth, dense shells were formed (Figure 2a,c) when the concentration of the oil-soluble surfactant dissolved in the disperse phase was low. However, no microcapsules were obtained when large amounts of oil-soluble surfactants were added, regardless of the kinds of surfactants used. Some of the microcapsules had macroholes in their shells when an oil-soluble surfactant was added at the threshold concentration, as indicated by the open triangles (△) in Table 4. Typical examples of microcapsules with macroholes are shown in Figure 2b,d. These results were precisely what we expected (i.e., the macroholes formed in places corresponding to where the oil-soluble surfactant had adsorbed instead of poly(E-MA)).

To evaluate the formation of macroholes quantitatively, we derived a theoretical equation for calculating the fraction of the surface of an emulsion droplet covered by poly(E-MA) and an oil-soluble surfactant as a function of the concentrations of poly (E-MA) and oil-soluble surfactant and the radius of the droplet. The derivation of the theoretical equation is given below. The competitive adsorption of poly(E-MA) and oil-soluble surfactant on the surface of an emulsion droplet was considered in the derivation. It is important to note that in the theory we assumed that poly(E-MA) and the oil-soluble surfactant do not interact with each other in the interfacial region and that they adsorb at the O/W interface independently.

Now, let us consider a unit oil droplet of O/W emulsion with radius r. An oil-soluble surfactant is dissolved in the oil phase (disperse phase) of the emulsion. Poly(E-MA) is dissolved in the water phase (continuous phase). The oil-soluble surfactant adsorbs on the surface of the emulsion droplet (i.e., adsorbs on the interface between the oil and water phases). The following equation is derived from the mass balance of the oil-soluble surfactant in the adsorption equilibrium state

$$\frac{C_{S,org,0}}{100} V_{org}\rho = \frac{C_{S,org,eq}}{100} V_{org}\rho + \Gamma_{S,eq} MA \qquad (1)$$

where $C_{S,org}$ is the concentration of oil-soluble surfactant in the oil phase in wt %, subscript 0 denotes the initial state and eq denotes the equilibrium state, $\Gamma_{S,eq}$ is the equilibrium adsorption amount of oil-soluble surfactant on the droplet surface in units of mol/m^2, ρ is the density of the solvent of the oil phase, M is the molecular weight of the oil-soluble surfactant; V_{org} denotes the volume of the oil phase, and A denotes the surface area of the emulsion droplet. V_{org} and A are both functions of r (i.e., $V_{org} = 4\pi r^3/3$ and $A = 4\pi r^2$). After substituting these relationships into eq 1 and simplifying, we obtain the following relationship among $C_{S,org,eq}$, $\Gamma_{S,eq}$, and r.

$$C_{S,org,eq} = C_{S,org,0} - \frac{300M}{\rho}\frac{\Gamma_{S,eq}}{r} \qquad (2)$$

Let us next consider the competitive adsorption of poly(E-MA) and oil-soluble surfactant on the surface of an emulsion droplet. We describe the adsorption equilibria of poly(E-MA) and oil-soluble surfactant at the oil/water interface with the Langmuir adsorption isotherm, which can be derived from either kinetic or thermodynamic considerations.[27] In our model, we used the Langmuir isotherm derived from kinetic considerations. In the kinetic derivation, adsorption is modeled as a dynamic equilibrium between adsorption to and desorption from the interface lattice. The adsorption rate of surfactant is taken to be proportional to the concentration of the surfactant in the bulk solution and the fraction of the surface lattice unoccupied by the surfactant. The desorption rate of surfactant is taken to be proportional to the fraction of the surface occupied by the surfactant. The dynamic equilibria of poly(E-MA) and oil-soluble surfactant are given as follows

$$k_{EMA}C_{EMA,aq}\theta_v = k_{EMA}'\theta_{EMA} \quad (3)$$

$$k_S C_{S,org}\theta_v = k_S'\theta_S \quad (4)$$

where k and k' are the adsorption and desorption rate constants, respectively; subscript EMA indicates poly(E-MA), and subscript S indicates oil-soluble surfactant; $C_{EMA,aq}$ is the concentration of poly(E-MA) in the continuous phase; θ_{EMA} and θ_S are the fractions of the surface of an emulsion droplet covered by poly(E-MA) and by oil-soluble surfactant, respectively; and θ_v is the fraction of the vacant interface. Among θ_{EMA}, θ_S, and θ_v, the following relationship holds:

$$\theta_{EMA} + \theta_S + \theta_v = 1 \quad (5)$$

The adsorption amounts of each surfactant on the interface are expressed by θ_{EMA} and θ_S as follows

$$\Gamma_{EMA} = \Gamma_{EMA}^{\infty}\theta_{EMA} \quad (6)$$

$$\Gamma_S = \Gamma_S^{\infty}\theta_S \quad (7)$$

where Γ^{∞} is the saturated adsorption amount of surfactant on the surface of an emulsion droplet. From eqs 3 – 7, we obtain the following well-known Langmuir adsorption isotherm in a binary component system.

$$\Gamma_{EMA,eq} = \frac{\Gamma_{EMA}^{\infty}K_{EMA}C_{EMA,aq,eq}}{1 + K_{EMA}C_{EMA,aq,eq} + K_S C_{S,org,eq}} \quad (8)$$

$$\Gamma_{S,eq} = \frac{\Gamma_S^{\infty}K_S C_{S,org,eq}}{1 + K_{EMA}C_{EMA,aq,eq} + K_S C_{S,org,eq}} \quad (9)$$

where K_{EMA} (= k_{EMA}/k_{EMA}') is the adsorption equilibrium constant of poly(E-MA) and K_S (= k_S/k_S') is that of oil-soluble surfactant. In these equations, $C_{EMA,aq,eq}$ can be regarded as the initial concentration of poly(E-MA), $C_{EMA,aq,0}$, because a sufficiently large amount of poly(E-MA) was dissolved in the continuous phase under the experimental conditions used in this study. By substituting eq 2 into eq 9 and solving for $\Gamma_{S,eq}$, we obtain an expression for $\Gamma_{S,eq}$ as a function of the radius of the emulsion droplet and the concentrations of oil-soluble surfactant and poly(E-MA). Subsequently, $\Gamma_{EMA,eq}$ can be calculated by substituting the calculated $\Gamma_{S,eq}$ and eq 2 into eq 8. The fraction of the surface of an emulsion droplet covered by poly(E-MA) and oil-soluble surfactant can be calculated by substituting the determined $\Gamma_{S,eq}$ and $\Gamma_{EMA,eq}$ into eqs 6 and 7, respectively. In these calculations, Γ_{EMA}^{∞}, Γ_S^{∞}, K_{EMA}, and K_S are unknown parameters. They were determined from interfacial tension measurement for a single adsorption system for all surfactants.

The relationship between interfacial tension and surfactant concentration is shown in Figure 3. The data were obtained for simple solutions of the oil-soluble surfactant in Isopar G or poly(E-MA) in water. As we can see from these plots, the interfacial tension decreased as the concentration of each surfactant was increased. To determine Γ_{EMA}^{∞}, Γ_S^{∞}, K_{EMA}, and K_S, we analyzed the data in Figure 3 with the following Langmuir–Szyszkowski equation[27]

$$\gamma = \gamma_0 - RT\Gamma_i^{\infty}\ln(1 + K_i C_{i,eq}) \quad (10)$$

where γ is the interfacial tension and γ_0 is that at $C_{i,eq} = 0$; R is the gas constant and T is temperature; subscript i denotes the surfactant being considered (i.e., i = S or EMA). The solid and broken lines in Figure 3 are the results calculated with eq 10. In the analysis, Γ_i^{∞} and K_i were determined by trial and error

(27) Prosser, A. J.; Franses, E. I. *Colloids Surf., A* **2001**, *178*, 1–40.

Table 5. Saturation Adsorption Amount, Γ_i^{∞}, and Adsorption Equilibrium Constant, K_i, of Each Surfactant on the Surface of the Emulsion Droplet

	Γ_i^{∞} (mol/m^2)	K_i (wt %$^{-1}$)
poly(E-MA)	2.0×10^{-6}	2.3×10^3
Solsperse17000	3.0×10^{-6}	1.7×10^4
SPAN85	3.7×10^{-6}	1.0×10^3

in order to show good correlation between the calculated line and the experimental data. The determined Γ_i^{∞} and K_i are listed in Table 5. They were used to calculate the fractions of the surface of an emulsion droplet covered by each surfactant, θ_i, as a function of the oil-soluble surfactant concentration and droplet radius.

The calculated results are shown in Figures 4 and 5. The effect of oil-soluble surfactant concentration on θ_i is shown in Figure 4. The value of $C_{EMA,aq,eq}$ used in the calculation was the same as for the initial concentration of poly(E-MA) under the conditions used to prepare the microcapsules given in Figure 2b,d (i.e., $C_{EMA,aq,eq} = C_{EMA,aq,0} = 1.67$ wt %). The radii of the emulsion droplets were adjusted to those of the microcapsules in Figure 2b,d (i.e., 9.4 μm for the Solsperse17000 system and 12.5 μm for the SPAN85 system). The calculated results for the Solsperse17000 system are indicated in Figure 4a by bold lines, and those for SPAN85 are indicated in Figure 4b by bold blue lines. As we can see from these lines, the values of θ_{EMA} for both oil-soluble surfactant systems at the threshold concentration of both oil-soluble surfactants are almost the same; θ_{EMA} is about 0.85 for both oil-soluble surfactants (indicated by the broken arrows in Figure 4a,b). These experimental and calculated results suggest the following hypothesis concerning the macrohole formation mechanism.

First, nuclei for the microcapsule shells are formed through a reaction between melamine–formaldehyde prepolymer and poly(E-MA). The nuclei are formed in the continuous phase and

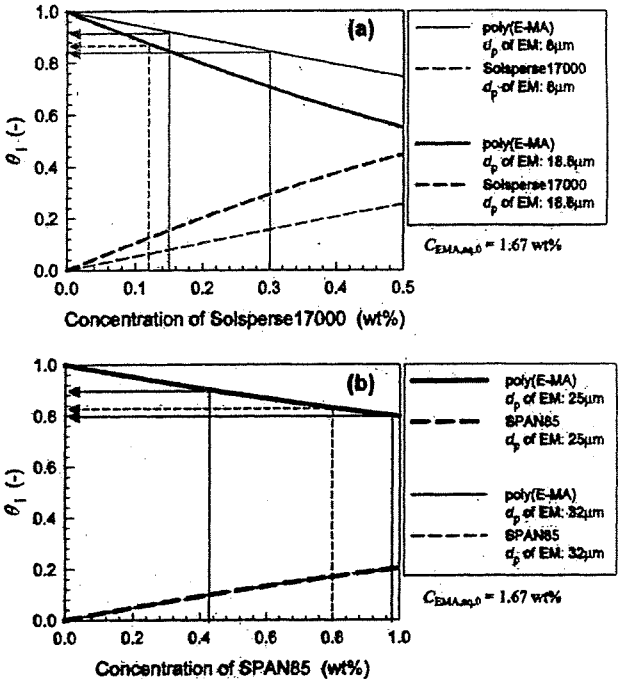

Figure 4. Relationship between θ_i and oil-soluble surfactant concentration. The oil-soluble surfactants were (a) Solsperse17000 and (b) SPAN85. In the legend, EM denotes emulsion, and d_p denotes the diameter of the emulsion droplet used as the microcapsule core.

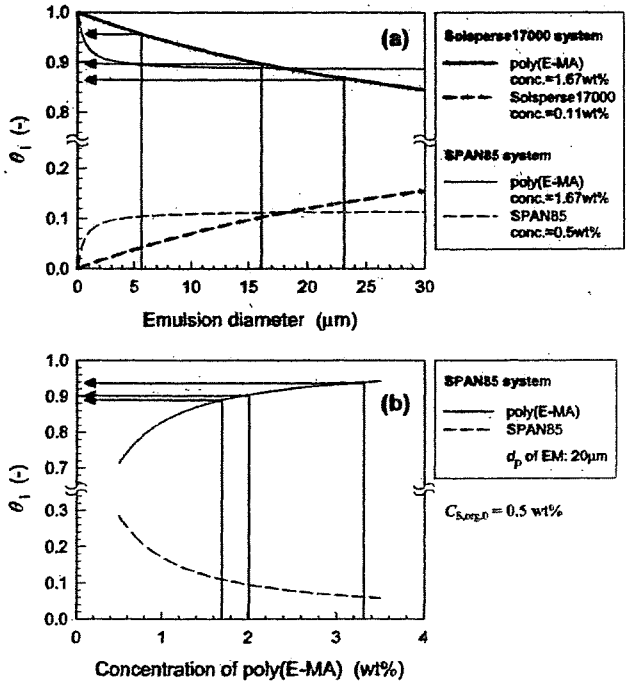

Figure 5. Relationships between (a) θ_i and the diameter of emulsion droplets used as the microcapsule cores and (b) θ_i and the concentration of poly(E-MA) in continuous phase III.

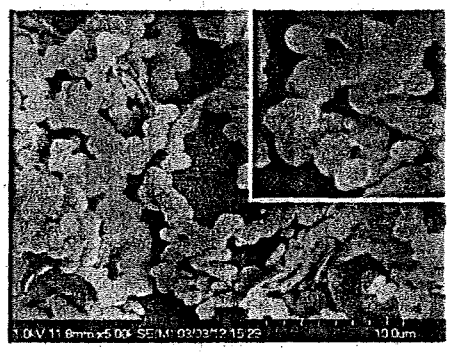

Figure 6. SEM image of microcapsule shells prepared under conditions of $C_{EMA,aq,0} = 1.67$ wt % and $C_{S,org,0} = 0.5$ wt %, where the oil-soluble surfactant used was Solsperse17000, and the emulsion droplet size was not controlled. In the upper right corner is an SEM image of the disklike shells.

on the surface of an emulsion droplet because poly(E-MA) molecules are dissolved in the continuous phase and are also adsorbed onto the droplet surface. The nuclei formed on the surface of an emulsion droplet grow through the reaction with melamine-formaldehyde prepolymer, the adhesion of nuclei deposited in the continuous phase, and the adhesion of other nuclei deposited on the droplet surface; then the precursors of the microcapsule shells are constructed on the droplet surface. The self-assembly of oil-soluble surfactant molecules adsorbed on the droplet surface occurs simultaneously. The microcapsule shell precursors grow parallel to the droplet surface, and disklike shells, similar to the ones in the upper right corner of Figure 6, are then formed on the droplet surface. The disklike shells no longer move on the droplet surface because they are too large. When θ_{EMA} is larger than 0.8, adjacent disklike shells connect with one another as they grow through the reaction with melamine−formaldehyde prepolymer and the adhesion of nuclei deposited in the continuous phase. When the number of disklike

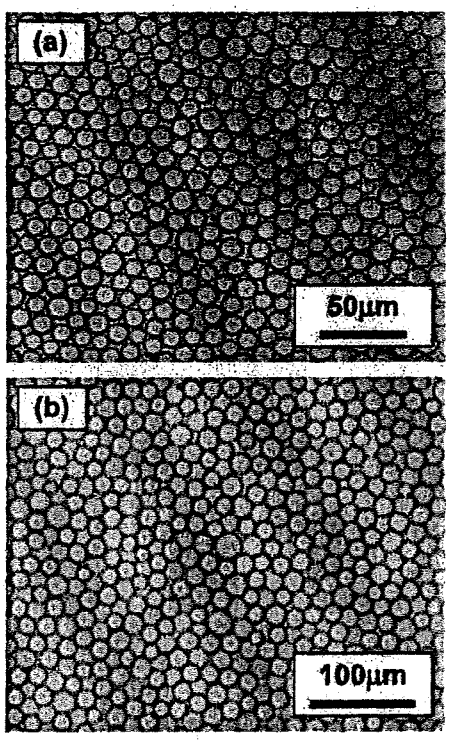

Figure 7. Optical microscopy images of the emulsions prepared by SPG membrane emulsification. The pore diameters of the SPG membrane were (a) 2.6 and (b) 4.8 μm.

shells formed on the droplet surface is sufficiently large (i.e., $\theta_{EMA} < 0.9$), microcapsules with smooth, dense shells are formed. If the number of disklike shells is somewhat small (i.e., $0.8 < \theta_{EMA} > 0.9$), then microcapsules with holes in their shells are formed. However, when θ_{EMA} is smaller than 0.8, adjacent disklike shells do not satisfactorily connect with one another. As a result, the microcapsules cannot retain their spherical form, as shown in Figure 6. If θ_{EMA} is much smaller, then no disklike shells are formed, which means that no microcapsules can be formed. To confirm the above hypothesis, we further investigated the effect of θ_{EMA} on the formation of the macroholes in the microcapsule shells.

We thought that if we adjusted the fraction of the droplet surface covered by poly(E-MA) to about 0.85 then only microcapsules with macroholes in their shells would be prepared. As we can see from Figure 5a, θ_{EMA} decreases as the droplet diameter increases. That is, we must use monodisperse emulsion droplets as the microcapsule core to precisely adjust the fraction of the droplet surface covered by the surfactants. Therefore, in the investigations described below, we used monodisperse emulsion droplets prepared by SPG membrane emulsification as the core.

The O/W emulsion prepared by SPG membrane emulsification is shown in Figure 7. As can be seen, the droplets were uniform in size. The average diameter was proportional to the pore diameters of the SPG membrane and about 5 times larger. The coefficient of variation (CV) values were almost 10%. We first investigated what effect the droplet diameters had on the preparation of holey microcapsules. The microencapsulation conditions are listed in Table 2, and the microencapsulation protocol is shown in Figure 1b. The arrows in Figure 5a indicate the θ_{EMA} corresponding to the droplet diameter for each type of emulsion used to prepare the microcapsules. The prepared microcapsules were strongly influenced by the droplet diameters,

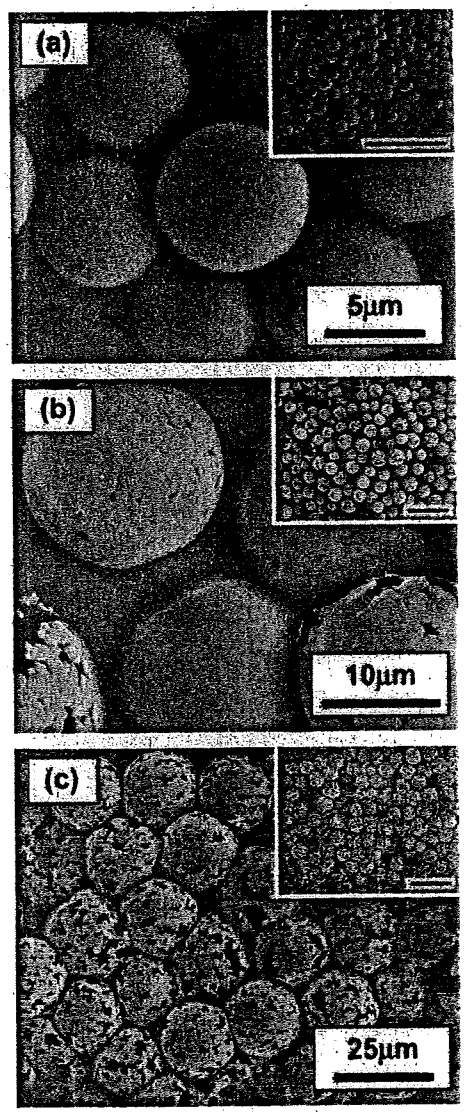

Figure 8. SEM images of microcapsules prepared using size-controlled emulsion droplets of various diameters. Preparation conditions: $C_{EMA,aq,0}$ = 1.67 wt % and $C_{S,org,0}$ = 0.11 wt %. the oil-soluble surfactant used was Solsperse17000, and the average droplet diameters were (a) 5.5, (b) 16.0, and (c) 23.0 μm. Overviews are shown in the insets, where the scale bars correspond to 50 μm.

as we expected from the theoretical calculations. The prepared microcapsules are shown in Figure 8. The microcapsules prepared using emulsion droplets with an average diameter of 5.5 μm (Figure 8a) had smooth complete shells. Those prepared using droplets with an average diameter of 16.0 μm consisted of ones with large holes and ones with small holes coexisting, as shown in Figure 8b. A careful study of the microcapsules in Figure 8b revealed that those with larger diameters had large holes whereas those with smaller diameters had small holes. The small differences in the diameters of droplets prepared by SPG membrane emulsification affected the size and quantity of macroholes in each microcapsule shell. Thus, if we could control the diameter of emulsion droplets (i.e., θ_{EMA}) more precisely, then we could control the diameter and quantity of macroholes. As additionally shown in Figure 8b, the diameters of microcapsules with small holes were about 16 μm. This result indicates that θ_{EMA} for 16-μm-diameter droplets is the critical θ_{EMA}. As we can see from Figure 5, the critical θ_{EMA} was nearly 0.90. Microcapsules prepared using droplets with an average diameter

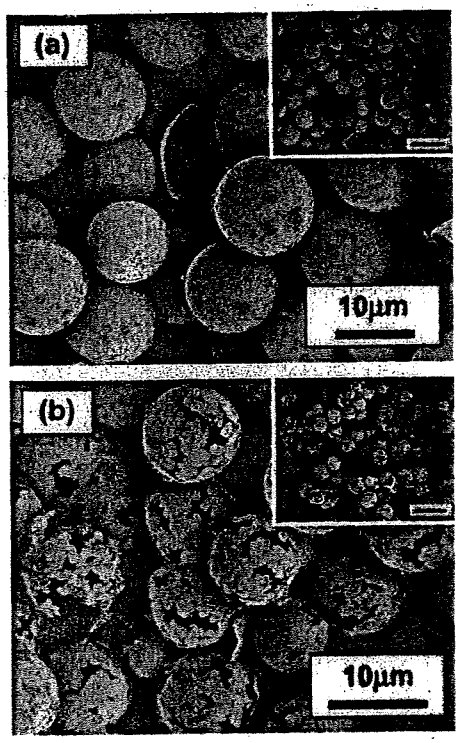

Figure 9. SEM images of microcapsules prepared with size-controlled emulsion droplets having different concentrations of Solsperse17000. Preparation conditions: $C_{EMA,aq,0}$ was 1.67 wt %, $C_{S,org,0}$ was (a) 0.15 and (b) 0.30 wt %, and the average droplet diameter was 8.0 μm. Overviews are shown in the insets, where the scale bars correspond to 20 μm.

of 23.0 μm are shown in Figure 8c. All of them had shells with macroholes. As can be seen from Figure 5, when the droplet diameter is 23.0 μm, θ_{EMA} is about 0.86. Therefore, only microcapsules with macroholes in the shells were formed.

Next, we investigated the effect of the concentration of Solsperse17000 on the formation of macroholes in the microcapsule shell. We used emulsion droplets with an average diameter of 8.0 μm in which 0.15 or 0.30 wt % of Solsperse17000 had been dissolved. The experimental conditions and microencapsulation protocol are listed in Table 2 and shown in Figure 1b, respectively. The calculated θ_{EMA} for each concentration of Solsperse17000 is indicated in Figure 4a by solid arrows. They indicate that θ_{EMA} is 0.92 for $C_{S,org,0}$ = 0.15 wt % and 0.84 for $C_{S,org,0}$ = 0.3 wt %. That is, the theoretical calculations suggest that microcapsules with complete shells will be prepared at $C_{S,org,0}$ = 0.15 wt % and microcapsules with macroholes will be prepared at $C_{S,org,0}$ = 0.3 wt %. Prepared microcapsules for both of these concentrations are shown in Figure 9. As expected from the calculated results, each of the microcapsules prepared at $C_{S,org,0}$ = 0.15 wt % had a complete shell and each of those prepared at $C_{S,org,0}$ = 0.3 wt % had a holey shell.

We also examined the preparation of microcapsules with macroholes in their shells by using SPAN85 as an oil-soluble surfactant. The theoretical calculation for the SPAN85 system shown in Figure 4b indicates that θ_{EMA} is weakly dependent on the concentration of SPAN85; that is, θ_{EMA} could be easily and precisely controlled by controlling the SPAN85 concentration. From the above-mentioned investigation of Solsperse17000, we expected that macroholes would appear when θ_{EMA} is in the range from 0.8 to 0.9. As shown by the thin red lines and the solid arrows in Figure 4b, the corresponding SPAN85 concentration range is 0.43−0.98 wt % when the diameter of an emulsion droplet is 32 μm. We prepared the microcapsules by using droplets

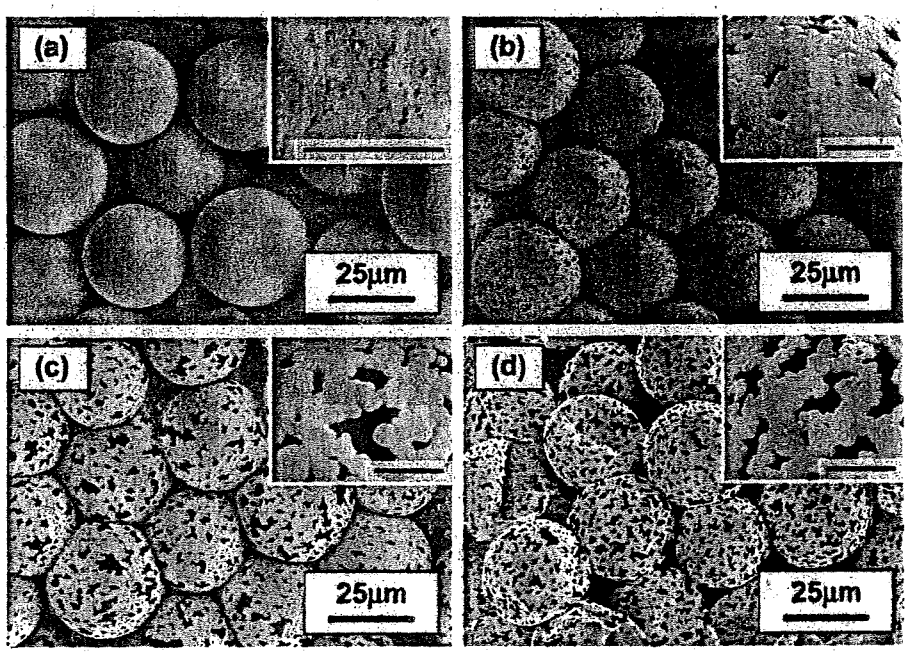

Figure 10. SEM images of the microcapsules prepared with size-controlled emulsion droplets containing different concentrations of SPAN85. Preparation conditions: $C_{EMA,aq,0}$ was 1.67 wt %; $C_{S,org,0}$ was (a) 0.43, (b) 0.50, (c) 0.60, and (d) 0.90 wt %; and the average droplet diameter was 32.3 μm. The insets are magnified views with the scale bars corresponding to 5 μm.

containing SPAN85 within this concentration range. The experimental conditions and microencapsulation protocol are listed in Table 3 and shown in Figure 1b, respectively. The droplets were prepared by SPG membrane emulsification. The average droplet diameter was 32 μm. Microcapsules enclosing the emulsion droplets containing 0.43, 0.50, 0.60, and 0.90 wt % SPAN85 are shown in Figure 10. As we expected, macroholes were formed in the shells of all of the microcapsules prepared in this investigation. In addition, the hole size increased with increasing SPAN85 concentration (i.e., the size of the macroholes could be controlled by adjusting the SPAN85 concentration). The holes in the shells of microcapsules prepared with 0.43 wt % SPAN85 were very small. From this result, we concluded that the critical concentration of SPAN85 for hole formation is 0.43 wt %. From the theoretical calculation, the corresponding θ_{EMA} was estimated to be 0.90, which agrees with the critical θ_{EMA} estimated for Solsperse17000.

Another parameter for controlling θ_{EMA} is the concentration of poly(E-MA) in continuous phase III. We examined the effect of $C_{EMA,aq,0}$ on the surface holes with the other conditions kept constant. As shown in Figure 5b, when the emulsion droplet diameter is 20 μm and the concentration of SPAN85 is 0.5 wt %, the concentration range of poly(E-MA) that provides a θ_{EMA} value of 0.8−0.9 is 0.8−2.0 wt %. We prepared microcapsules according to this calculated result. The experimental conditions and microencapsulation protocol are listed in Table 3 and shown in Figure 1b, respectively. The average diameter of the emulsion droplets used was 18.3 μm. The prepared microcapsules are shown in Figure 11. As expected, the microcapsules prepared with 1.67 wt % poly(E-MA) had macroholes, and those prepared with 3.33 wt % had no holes. In addition, when $C_{EMA,aq,0}$ was 2.0 wt % (i.e., θ_{EMA} was the critical value of 0.90), very small holes were formed in the microcapsule shells.

We also investigated the effect of the concentration of melamine−formaldehyde prepolymer in continuous phase III, which would not affect θ_{EMA}, on the surface holes with other conditions kept constant. The experimental conditions and prepared microcapsules are shown in the Supporting Information (Figure S2). We found that the morphology of the microcapsule shell (e.g., the size and density of the macroholes) was hardly affected by the prepolymer concentration. This result agrees with our theoretical considerations.

We conclude from these experimental and theoretical investigations that cross-linked polymelamine microcapsules with macroholes in their shells can be prepared by controlling the fraction of the emulsion droplet surface covered by poly(E-MA) in the presence of an additional oil-soluble surfactant. The formation of macroholes in the microcapsule shells seems to be related to the oil-soluble surfactant adsorbed on the droplet surface, and these surfactant molecules seem to self-assemble at the surface during shell formation. We again note that, in our model, we assumed that poly(E-MA) and the oil-soluble surfactant do not interact with each other in the interfacial region and that they adsorb at the O/W interface independently. However, they might be in association equilibrium with each other, and the associated complex might adsorb on some sites in the interface. It may be possible to obtain a rigorous relationship between the ratio of the hole area of the surface of the microcapsules and the ratio of components adsorbed on the interface by applying a competitive adsorption isotherm model derived for the multicomponent system in which the adsorption of an associated complex is also considered. Although the association between polymer and surfactant has been investigated in previous studies, most of them discussed the interactions between polymer and surfactant coexisting in the same phase.[28] More knowledge about the interaction between polymer and surfactant in the oil/water interfacial region would be useful.

Application of Microcapsules with Macroholes in Their Shells. *Release of Core Material from Holey Microcapsules.* As an example of the applications of microcapsules with macroholes in their shells, we examined the controlled release of encapsulated material. One would expect the release rate to increase with the

(28) (a) Jones, M. N. *J. Colloid Interface Sci.* **1967**, *23*, 36–42. (b) Folmer, B. M.; Kronberg, B. *Langmuir* **2000**, *16*, 5987–5992. (c) Touhami, Y.; Rana, D.; Neale, G. H.; Hornof, V. *Colloid Polym. Sci.* **2001**, *279*, 297–300. (d) Goddard, E. D. *J. Colloid Interface Sci.* **2002**, *256*, 228–235.

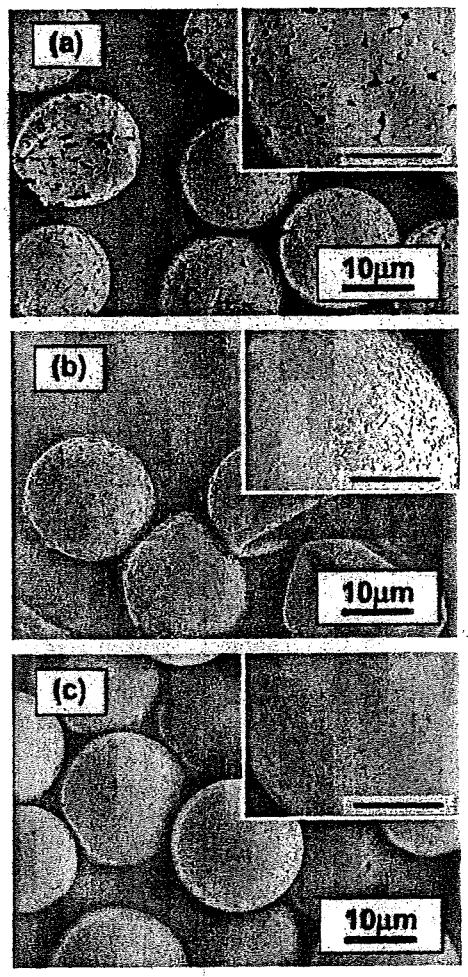

Figure 11. SEM images of microcapsules prepared with different concentrations of poly(E-MA). Preparation conditions: $C_{EMA,aq,0}$ was (a) 1.67, (b) 2.0, and (c) 3.33 wt % and $C_{S,org,0}$ was 0.5 wt %. SPAN85 was used as an oil-soluble surfactant. The emulsion droplets were size-controlled ones prepared by SPG membrane emulsification. The average droplet diameter was 18.3 μm. The insets are magnified views with the scale bars corresponding to 5 μm.

size of the macroholes. We investigated the release behavior by using holey microcapsules prepared from emulsion droplets containing a small amount of blue dye (oil blue N) and 0, 0.43, 0.5, and 0.6 wt % SPAN85. The average diameter of the emulsion droplets was 32.3 μm. Microcapsules prepared without SPAN85 had smooth, complete shells whereas those prepared with SPAN85 had holey shells. For each SPAN85 concentration, the holes were nearly the same size as those in the microcapsules prepared with the same SPAN85 concentration in Figure 10. The release behavior was evaluated by measuring the concentration of oil blue N that was eluted from the microcapsule into the elutriant (ethanol). The results are shown in Figure 12a, where C_{dye} denotes the concentration of oil blue N in the elutriant. It is clearly shown in Figure 12a that the release rate becomes as high as the concentration of SPAN85 in the encapsulated emulsion droplet increase. The release behavior of hole-free microcapsules ([SPAN85] = 0 wt %) is obviously different from that of holey ones. Hardly any oil blue N was released in the first 300 s. However, once release began, it was almost completed by 1200 s. The reason that such a specific release profile was observed was clearly revealed in an SEM photograph of the hole-free microcapsules after the controlled release experiment. As shown in Figure 12b, almost all hole-free microcapsules were crushed

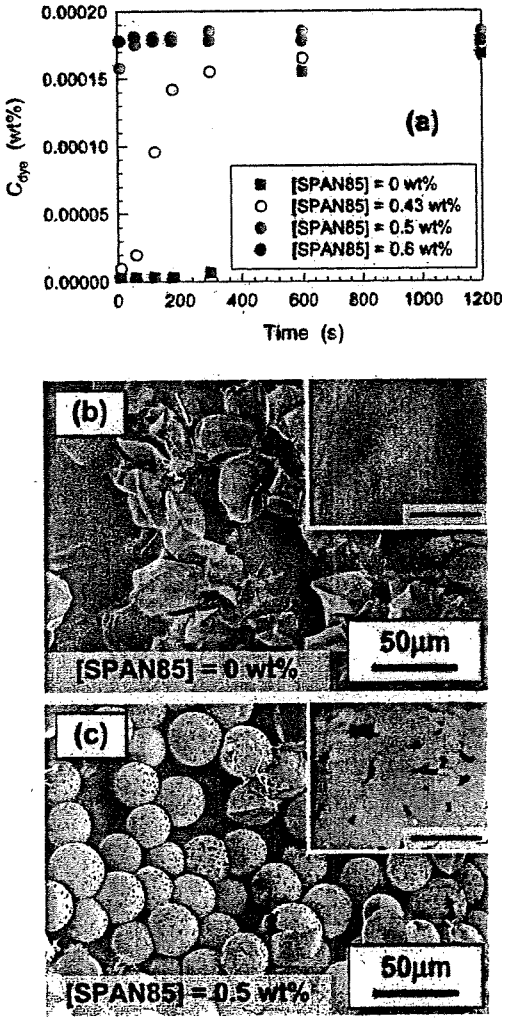

Figure 12. Controlled release behavior of microcapsules with and without holes in their shells. (a) Time course of the concentration of oil blue N released from the microcapsules. (b, c) SEM images of the microcapsules after elution; average droplet diameter was 32.3 μm, and SPAN85 concentration in the microencapsulated Isopar G was (b) 0 and (c) 0.5 wt %. The insets are magnified views with the scale bars corresponding to 5 μm.

and had slight cracks in their shells. In the early stage, ethanol entered the microcapsule through the shells. Because the solvent of the core material (Isopar G) could not penetrate the shells, the hole-free microcapsules burst after 300 s as a result of ethanol penetration into the cores and the formation of cracks in the shells. The materials encapsulated in the microcapsules were then eluted through the cracks. At that time, ethanol could not flow into the microcapsules because of the pressure difference inside and outside the microcapsules. Therefore, the hole-free microcapsules were crushed. However, the microcapsules with holes were not crushed during the elution of the core material. An example of an SEM photograph of holey microcapsules after the controlled release experiment is shown in Figure 12c. Because the inflow of ethanol and the outflow of the core material through the holes occurred simultaneously, the holey microcapsules were hardly crushed. In addition, as shown in Figure 12c, the holey microcapsules were not crushed after filtration and drying with ethanol. Dried holey microcapsules

(29) Daiguji, H.; Makuta, T.; Kinoshita, H.; Oyabu, T.; Takemura, F. *J. Phys. Chem. B* **2007**, *111*, 8879–8884.

contain air, so we can use them as templates for monodisperse size-controlled microcapsules encapsulating gaseous cores, which could be fabricated if we could successfully close the holes in the dried microcapsules. Microcapsule-encapsulating gaseous cores will be useful for many applications, including the weight reduction of materials and thermal and acoustical insulation (e.g., diagnostic ultrasound contrast agents).[29] The fabrication of microcapsules encapsulating gaseous cores is a topic for future work.

Fabrication of Microcapsules Encapsulating Aqueous Solution. As shown in Figure 12a, the core material in the holey microcapsules was quickly removed and replaced by ethanol. We expected that this ethanol substituting for the original core material could also be removed easily and replaced by water. That is, we thought it would be easy to obtain holey microcapsules containing an aqueous solution. If the holes in the shells of the microcapsules containing aqueous solution can be successfully closed, then microcapsules encapsulating aqueous solution can be fabricated. We thought that the holes could be closed by additional microencapsulation of the holey microcapsules containing aqueous solution as the cores. To demonstrate the feasibility of fabricating microcapsules with double-layer shells, we added reactive water-soluble dye to the continuous phase used for the additional microencapsulating process. We chose to use reactive blue 160 as a reactive water-soluble dye because it has both triazine and sec-amine units and thus can react with melamine–formaldehyde prepolymer. Therefore, the shells of the microcapsules synthesized in aqueous solution containing reactive blue 160 become blue. We can easily recognize the formation of the additional shells on the holey microcapsules. In addition, we used emulsion droplets including a small amount of oil-soluble red dye (oil red O) to confirm the complete removal of the oily core from the holey microcapsules. The additional microencapsulation was performed according to the process shown in Figure 1a and the conditions shown in Table 1. As continuous phase I, we used an aqueous solution with 2.5 wt % poly(E-MA) and 0.1 wt % Reactive Blue 160 dissolved in it. Instead of the disperse phase, we used a suspension of holey microcapsules prepared from emulsion droplets with 0.5 wt % SPAN85 and then washed with ethanol and distilled water to replace the core material with water. The mass fraction of the microcapsules in the suspension was about 75%. The prepared microcapsules were separated from the continuous phase and washed with distilled water. They were filtered and dried to enable us to observe the morphology by FE-SEM. The holey microcapsules and the resultant double-layer microcapsules encapsulating the aqueous solution are shown in Figure 13. Figure 13a is an SEM photograph of the holey microcapsules, which are the original starting blocks for the double-layer microcapsules encapsulating the aqueous solution. As shown in the upper inset, submicrometer-sized macroholes were formed in the shell of each microcapsule. The original holy microcapsules with the core material replaced by water were microencapsulated again. An SEM photograph of the obtained double-layer microcapsules is shown in Figure 13b. It is clear that the macroholes were successfully closed. The upper inset in Figure 13b is an SEM photograph of the crosssection of the microcapsule. This image confirms that the microcapsule had a single core. The lower insert in Figure 13b is a photograph of a dried sample. This image clearly shows that the microcapsule is blue. That is, the additional shell was formed on the surface of the original microcapsule and closed the holes. Figure 13c shows the suspensions of microcapsules. The microcapsules in the left test tube are the original ones encapsulating Isopar G with oil red O dissolved in it. Because the density of Isopar G (7.49×10^5 g/m^3) was less than that of water, the microcapsules floated. The microcapsules with their core material replaced by water are in the middle test tube. The color of these microcapsules is white instead of red, which indicates that the oily core in the original microcapsules was completely removed. In addition, the microcapsules in the middle tube sank in water, which means that the oily core had been replaced by water. The double-layer microcapsules with closed holes are in the right test tube. They also sank in water (i.e., the aqueous solution was encapsulated in the microcapsules). This confirms that a holey microcapsule can be used as a template for fabricating a microcapsule encapsulating hydrophilic compounds. It should be noted that macroholes slightly larger than those shown in Figure 13a were not completely closed and that nanosized holes remained in the microcapsule shells after the additional microencapsulation. A microcapsule that contains an aqueous solution and has a shell with tiny holes is potentially applicable as a bioreactor. The

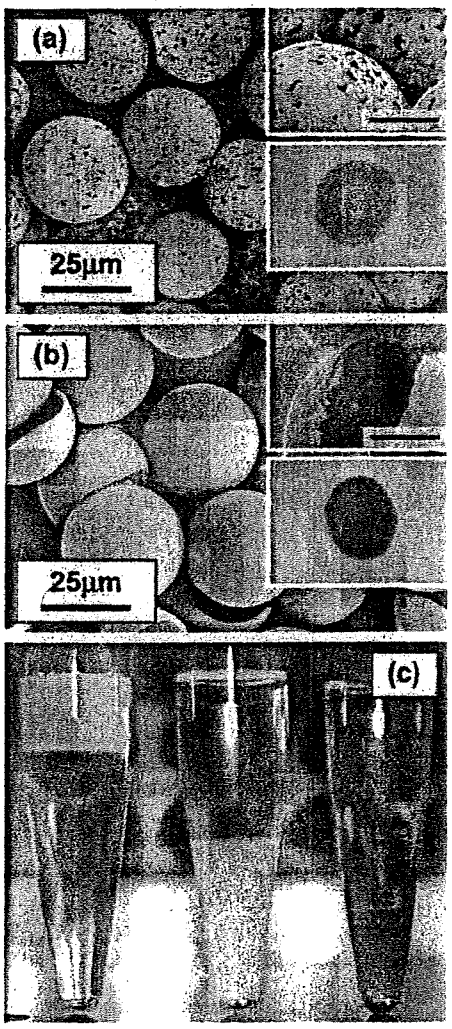

Figure 13. Microcapsules encapsulating aqueous solution after additional microencapsulation of the holey microcapsules. (a) Original microcapsules encapsulating aqueous solution; holey microcapsules were prepared with emulsion droplets having an average diameter of 32.3 μm and containing 0.5 wt % of SPAN85 and a small amount of a red dye (oil red O). (b) Microcapsules encapsulating an aqueous solution. The upper insets in panels a and b are magnified views with the scale bars corresponding to 10 μm, and the lower ones are photographs of filtered samples. (c) Suspensions of the microcapsules in distilled water. (Left) original microcapsules shown in panel a, (middle) holey microcapsules with their core material replaced by water, and (right) microcapsules encapsulating the aqueous solution shown in panel b.

macroholes in the shell of the original microcapsule should allow free diffusion of a living cell or a bacillus into the microcapsule. Then, the macroholes could be closed by the additional microencapsulation. The nanosized holes remaining after the additional microencapsulation should prevent a living cell or bacillus from leaving the microcapsule and should also allow free diffusion of gases, nutrients, and wastes. With the aim of making a bioreactor, we are planning to perform further investigations into the fabrication of microcapsules containing an aqueous solution suspending biocatalysts and having shells with nanosized holes.

Conclusions

We described the preparation of cross-linked polymelamine microcapsules with macroholes in their shells by a phase-separation method. The macroholes were formed by utilizing the competitive adsorption of a water-soluble polymeric surfactant and an oil-soluble surfactant on the surface of an emulsion droplet used as the capsule core. Theoretical calculations based on the competitive adsorption of surfactants on the surface of an emulsion droplet were used to explain the formation of macroholes in microcapsule shells. The theoretical calculations revealed that the fraction of the droplet surface covered by poly(E-MA) depended on the concentrations of poly(E-MA) and the oil-soluble surfactant and the diameter of the emulsion droplet. By comparing the properties of prepared microcapsules with the calculated results, we found that for poly(E-MA) the critical degree of surface coverage needed to fabricate holey microcapsules was about 0.90. By controlling the concentrations of poly(E-MA) and the oil-soluble surfactant and the droplet diameter according to the calculated results, we successfully prepared only microcapsules with macroholes. The size and quantity of macroholes could be controlled by adjusting the fraction of the droplet surface covered by poly(E-MA). We conclude from the experimental and theoretical investigations that the macroholes formed in microcapsule shells resulted from the adsorption and self-assembly of the oil-soluble surfactant on the droplet surface during the formation of the shells of cross-linked polymelamine microcapsules.

The applications of microcapsules with macroholes in their shells were also investigated. Controlling the hole size allowed us to control the release rate of the core material. Microcapsules with macroholes have the potential to be used in controlled release applications. We also found that they were not crushed when the core material was being replaced. Microcapsules containing an aqueous solution were fabricated by using the microcapsules with macroholes as templates. The macroholes in the shells were successfully closed by an additional microencapsulation. Thus, microcapsules with macroholes in their shells can also be used as templates for fabricating microcapsules containing hydrophilic compounds, which could be used as bioreactors.

Acknowledgment. This work was supported in part by the New Energy and Industrial Technology Development Organization's (NEDO's) "Nanotechnology Materials Program—Encapsulation of Functional Nano-particles Project" based on funds provided by the Ministry of Economy, Trade, and Industry, Japan (METI) and administered by the Japan Chemical Innovation Institute (JCII).

Supporting Information Available: Detailed schematic explanation of SPG membrane emulsification followed by the microencapsulation process and microcapsules prepared with different concentrations of melamine–formaldehyde prepolymer with the other conditions constant. This material is available free of charge via the Internet at http://pubs.acs.org.

LA800758D

Colloid Polym Sci
DOI 10.1007/s00396-008-1924-9

ORIGINAL CONTRIBUTION

Effects of dispersion stabilizer and reaction solvent on forming monodisperse polystyrene microspheres by dispersion polymerization

Takuro Nakashima · Tsutomu Ono

Received: 25 June 2008 / Accepted: 26 August 2008

Abstract We used poly(aspartic acid) (PAsp) synthesized by ion exchange with sodium polyaspartate (PAspNa) as a dispersion stabilizer. PAsp improved the dispersion stability and the solubility in the medium for dispersion polymerization. The effects of the stabilizer hydrophobicity on particle formation, conversion, particle diameter, and its distribution of polystyrene microspheres were investigated by using both biodegradable polymers as a dispersion stabilizer. According to these results, we concluded that the polymerization rate of the styrene with PAsp was higher than that of styrene with PAspNa. That is why, smaller and more monodisperse microspheres were prepared with PAsp, compared to those with PAspNa.

Keywords Poly(aspartic acid) · Dispersion polymerization · Monodisperse particle · Biodegradable polymer · Polystyrene

Introduction

Dispersion polymerization is one of the major techniques for the preparation of monodisperse polymer microspheres [1–6]. In dispersion polymerization, monodisperse microspheres are formed in the presence of appropriate polymer dispersion stabilizer such as poly(*N*-vinylpyrrolidone), polyacrylic acid (PAA), and polyethylenimine [7, 8]. However, all commercial dispersion stabilizers used in dispersion polymerization are so far not biodegradable. In general, these water-soluble polymers are difficult to recover from polymer solution. Therefore, these nonbiodegradable dispersion stabilizers cause contamination of polymer microsphere surface and waste-water treatment of polluted water. Furthermore, these are made from fossil fuels. When we thought about sustainable society, cutting our dependence on fossil fuels is essential.

Sodium polyaspartate (PAspNa) synthesized by polycondensation of L-aspartic acid (L-Asp) is one of the typical hydrophilic biodegradable polymers [9, 10]. Since PAspNa is made from plant-derived materials and has biocompatibility, this polymer can be used in medical field, cosmetics, and foods. Thus, we studied dispersion polymerization with PAspNa as a dispersion stabilizer and synthesized monodisperse polystyrene microspheres with PAspNa as a dispersion stabilizer. The particle diameter ranged between 0.25 and 2.3 μm, and the particle size distribution was about 7.7%.

In this work, we synthesized poly(aspartic acid) (PAsp) by ion exchange with PAspNa. Although PAsp is also a typical hydrophilic biodegradable polymer, the solubility in water is lower than PAspNa due to weak-acid polyelectrolyte. We investigated the effect of the stabilizer hydrophobicity on the particle formation, conversion, particle size, and the distribution of polystyrene particles.

Experimental

Materials

All chemicals were purchased from Wako Pure Chemical Industry. Styrene (99%, with 3.0×10^{-3}% 4-tert-butylpyrocatechol stabilizer) was distilled under reduced pressure in a nitrogen atmosphere to remove the inhibitor. 2,2′-Azobis

T. Nakashima · T. Ono (✉)
Department of Material and Energy Science,
Graduate School of Environmental Science, Okayama University,
3-1-1 Tsushima-Naka,
Okayama 700-8530, Japan
e-mail: tono@cc.okayama-u.ac.jp

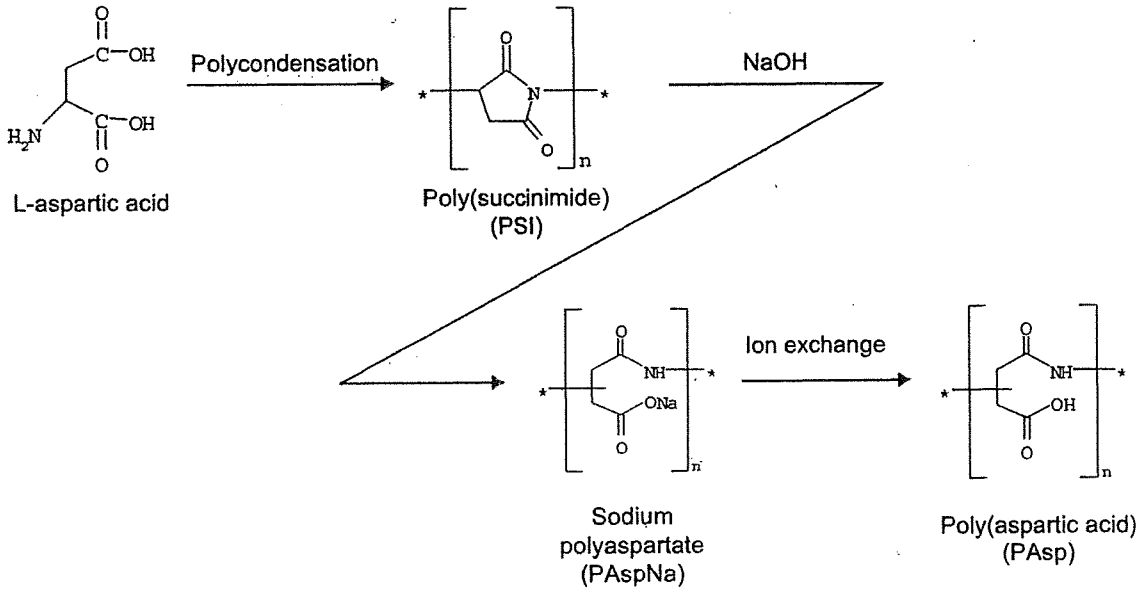

Scheme 1 Synthesis of PSI, PAspNa and PAsp

(isobutyronitrile) (AIBN) was purified by recrystallization from methanol. Water used as a polymerization solvent was purified with a Millipore Milli-Q water purification system.

Synthesis of polysuccinimide

Polysuccinimide (PSI) was synthesized by polycondensation of L-Asp (46.6 g) using phosphoric acid (19.8 g) as a catalyst at 453 K for 8 h. Then, the products were purified, and the weight-average molecular weights were determined by gel permeation chromatography (GPC) as previously reported [11]. The determined molecular weight of PSI was 4.25×10^4. Proton nuclear magnetic resonance (^{1}H NMR) spectra were measured with a JEOL FT NMR System JMN-AL300 (Scheme 1).

Synthesis of PAspNa

PAspNa was prepared by hydrolysis of PSI as already reported [11]. The molecular weight of PAspNa was 6.0×10^4, calculated from the molecular weight of PSI. The chemical structure of PAspNa was confirmed by Fourier transform infrared spectroscopy (FT-IR; KBr method). ^{1}H NMR spectra were measured with a JEOL FT NMR System JMN-AL300.

Synthesis of PAsp

PAspNa was dissolved in purified water, and an ion-exchange resin (Lewatit MonoPlus S100H) was added into the solution. After 24 h, the solution was concentrated under reduced pressure at 313 K [12]. The remaining solution was added into acetone to precipitate PAsp and which was recovered by filtration. The conversion from PAspNa to PAsp was confirmed by FT-IR (KBr method). The ion-exchange efficiency was calculated from natrium ion concentration. The natrium ion concentration was measured with an ion meter (DKK-TOA, IM-55G).

Microsphere preparation

Polystyrene microspheres were prepared by dispersion polymerization under the conditions listed in Table 1. Prepared microspheres were observed with a Hitachi S-3500N scanning electron microscope (SEM), and the average diameter and coefficient of variation (CV) were analyzed from the SEM images by WinRoof (Mitani, Ver.3.53). The average diameter and CV were defined by counting at least 200 individual microspheres from SEM image. The CV was calculated from the average diameter and standard deviation.

Table 1 Recipe for the preparation of monodisperse polystyrene microspheres

Ingredients	Units	Values
Styrene	g	1.35
AIBN	g	0.107
Dispersion stabilizer	g	0.15
Aqueous ethanol solution	Ml	45

343 K; 6 h; N_2; in flask with stirring rate, 360 rpm
AIBN 2,2'-Azobisisobutyronitrile

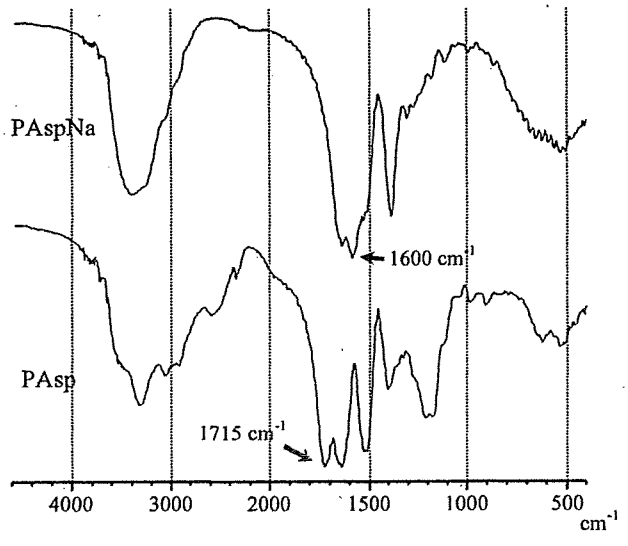

Fig. 1 FT-IR spectra of PAspNa and PAsp

Measurements of time course of conversion, particle diameter and its distribution, and particle numbers

A small amount of polymerization solvent with PAspNa or PAsp was withdrawn at different polymerization intervals. The samples were dissolved in methanol with a small amount of 4-tert-butylcatechol to terminate the polymerization. The concentrations of residual styrene monomer dissolved in methanol solution were determined by HPLC to estimate the conversion. The samples were also measured with the SEM to determine the particle diameters of the prepared microspheres at different polymerization intervals. Particle numbers were calculated from the conversion and particle diameters.

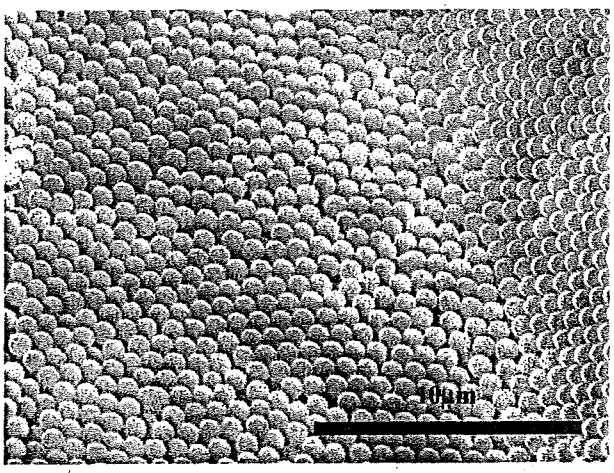

Fig. 2 SEM image of polymeric microspheres synthesized with PAsp. Volume fraction of EtOH=60 vol.%

Results and discussion

Characterization of synthesized PSI, PAspNa, and PAsp

The chemical structures of synthesized PSI and PAspNa were characterized by ^{1}H NMR as previously reported [11, 13].

The residues of synthesized PAspNa and PAsp were determined by FT-IR [12, 14, 15]. Figure 1 shows FT-IR spectra of PAspNa and PAsp. Attention was directed to the frequency of the carboxylate group band in order to investigate the preparing of the PAsp. The spectrum of PAspNa shows a large absorbance at 1,610 cm^{-1} assigned to the carboxylate anion (–COO$^-$). Meanwhile, the carboxylate anion band disappeared in the spectrum of PAsp. At

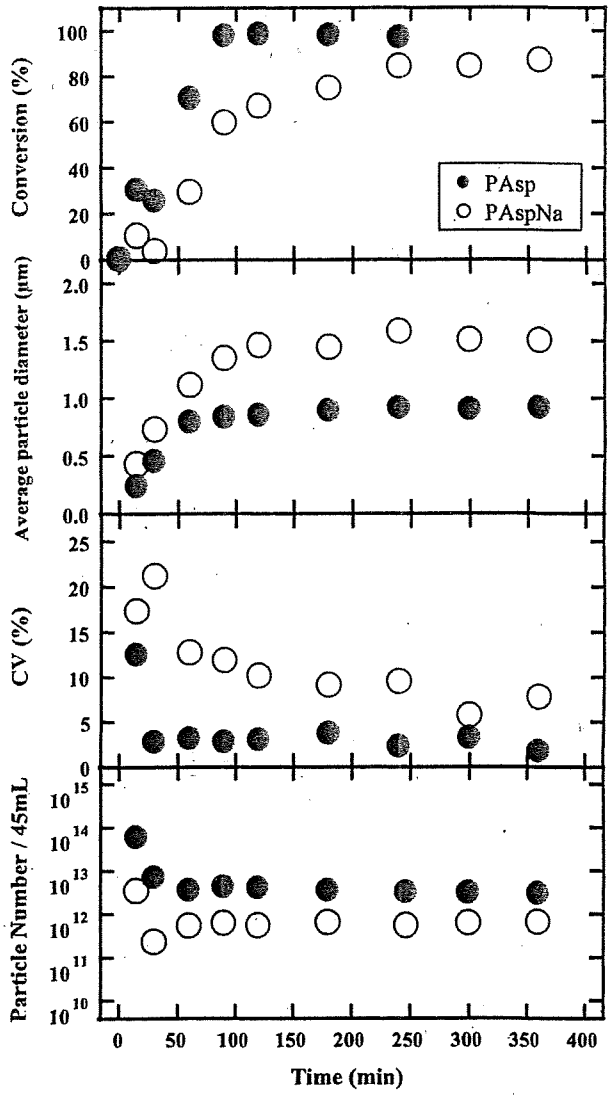

Fig. 3 Time course of conversion, particle diameter, CV, and particle number. Concentration of dispersion stabilizer = 3.33 mg/mL. Volume fraction of EtOH=60 vol%

the same time, a new band appeared at 1,720 cm^{-1}. This was assigned to the carboxylate group (–COOH).

In addition, the ion-exchange efficiency was calculated from the natrium ion concentration. It was measured before and after ion exchange of PAspNa solution. As a result, the natrium ion concentration after an ion-exchange process was very low. It was considered that almost all natrium ions of PAspNa were exchanged into hydrogen ions.

Thus, it was concluded that PAsp was successfully prepared from PAspNa by ion-exchange resin.

Kinetics of dispersion polymerization of styrene with PAspNa or PAsp

Figure 2 shows the SEM image of the polystyrene microspheres prepared with PAsp in an EtOH/water mixture with 60 vol.% EtOH. The particle diameter was approximately 0.91 μm. The CV was approximately 3.1%. The monodisperse polystyrene microspheres were clearly observed. This result indicates that PAsp acts as a dispersion stabilizer.

Figure 3 shows the time courses of styrene conversion, particle diameter, CV, and particle numbers of polystyrene microsphere in the dispersion polymerization using PAspNa or PAsp. The concentration of dispersion stabilizer was 3.4 mg/ml.

The final conversion with PAspNa is 87%. Meanwhile, the final conversion with PAsp came up to about 100%. Furthermore, the polymerization rate of styrene with PAsp was higher than that with PAspNa. The polymerization mechanism observed is similar to that in our previous studies concerning dispersion polymerization [16, 17].

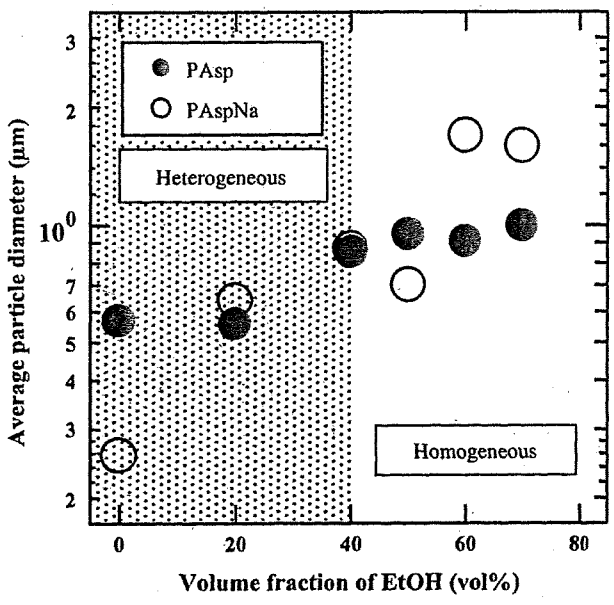

Fig. 4 Effect of EtOH volume fraction on particle diameter. Concentration of dispersion stabilizer = 3.33 mg/mL

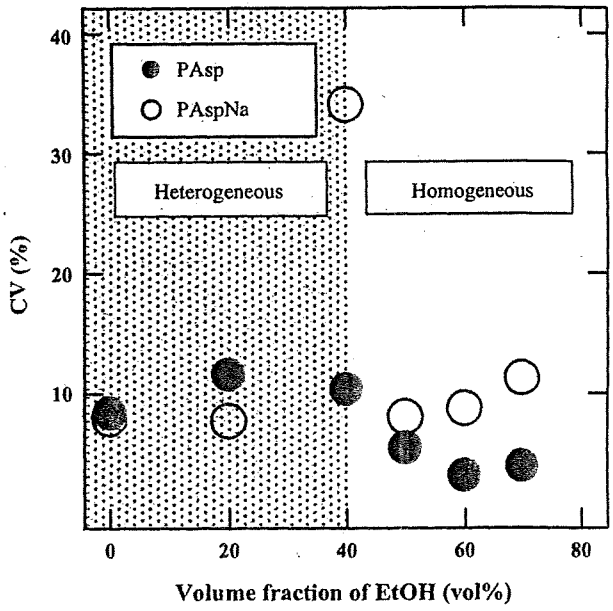

Fig. 5 Effect of EtOH volume fraction on CV. Concentration of dispersion stabilizer = 3.33 mg/mL

The diameter of particle prepared with PAsp was smaller than that prepared with PAspNa. In addition, the growth rate of microspheres with PAsp was faster than that with PAspNa.

The CVs obtained with PAsp and PAspNa decreased with time, and the CV obtained with PAsp was smaller than that with PAspNa.

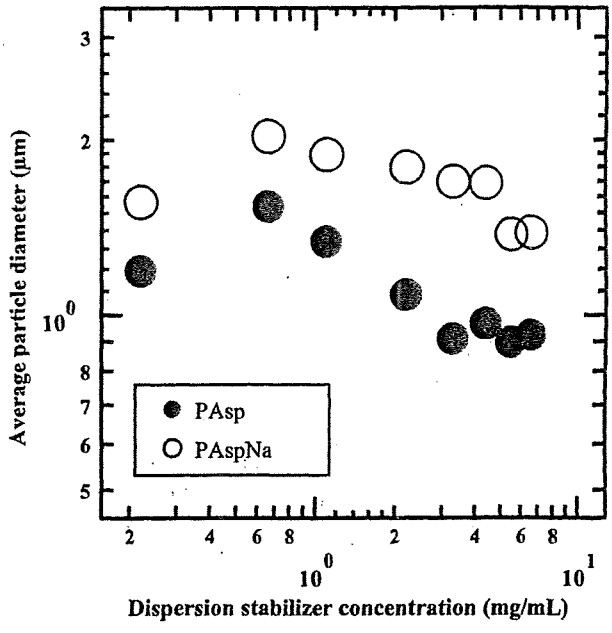

Fig. 6 Effect of dispersion stabilizer concentration on particle diameter. Volume fraction of EtOH = 60 vol%